LBL-15240
Preprint c.2

Lawrence Berkeley Laboratory
UNIVERSITY OF CALIFORNIA

Materials & Molecular Research Division

Submitted to Wear

THE PLATELET MECHANISM OF EROSION OF DUCTILE METALS

Alan V. Levy

May 1982

Prepared for the U.S. Department of Energy under Contract DE-AC03-76SF00098

DISCLAIMER

LBL-15240

THE PLATELET MECHANISM OF EROSION OF DUCTILE METALS

Alan V. Levy

Materials and Molecular Research Division
Lawrence Berkeley Laboratory
University of California
Berkeley, California 94720

Research sponsored by the Department of Energy under DOE/FEAA 15 10 10 0, Advanced Research and Technical Development, Fossil Energy Materials Program, Work Breakdown Structure Element LBL-3.5 and under Contract No. DE-AC03-76SF00098

ABSTRACT

A platelet mechanism of erosion for ductile metals is defined, set in historical perspective, and evidence of its validity is presented. The effects of various mechanical properties of metals on their erosion by particles carried in gas streams is reported and related to the proposed erosion mechanism. Elevated temperature erosion and combined erosion-corrosion is also discussed, in the context of the defined mechanism of erosion.

The data presented indicates that erosion should be thought of in a different manner from that proposed in the bulk of the literature of the 1960's and 1970's. Properties of alloys such as ductility, strain hardening coefficient and some thermal properties that have not previously been considered in selecting alloys for erosion service are the important selection factors, particularily ductility. Hardness and strength, generally used in the past to guide material selection, do not relate to erosion resistance in the manner prescribed to them in the older erosion literature. Their use in selecting alloys needs to be greatly modified.

INTRODUCTION

Structural metals have had surface material removed in service as the result of erosion by small, solid, impacting particles for a long time. Through the years particular engineering problems have arisen that temporarily intensified erosion research. Among them have been catalytic cracker erosion from catalyst pellets, turbine engine compressor blade erosion from sand ingestion in helicopter engines and char particle erosion in coal gasifiers. Until 1958 much of the work carried out to obtain erosion information was empirical. In 1958 Finnie developed an analytical model to attempt to predict erosion rates that was based on the assumption that the mechanism of erosion was micro-machining.[1] Based on the primary assumption that the eroding particles cut swaths of metal away from the alloy as their tips translated along the eroding surface, the basis for the analytical model was an equation of motion of the tips of the particles. By analytically describing the path of the particle and assuming that "the volume (of metal) removed is the product of the area swept out by the particle tip and the width B of the cutting face" as quoted in a more recent treatment of the model by Finnie and McFadden he accounted for metal removal by the erosion process.[2]

This basic assumption of micro-machining of the target metal by the tips of the eroding particles has pervaded the literature almost to the present day. The model was faulted by not being able to predict several important aspects of the measured erosion loss. These include the accurate effect of particle velocity (its exponent in the model), the occurence of considerable weight loss near an impingement angle of 90° (model predicts no erosion at 90°) and the impingement angle where maximum erosion occurs (experimental curves had to be moved to make the measured angle and the predicted angle coincide). In spite of its shortcomings the micro-machining mechanism was used by essentially all investigators in the field until about 1980. Since then, however, a mounting body of evidence is demonstrating that micro-machining is <u>not</u> the mechanism by which ductile structural metals erode. This evidence will be presented in this review.

The other major consideration in the erosion of ductile metals that has been widely accepted for many years it the effect of hardness/strength. Finnie published a report in 1967 that contained a curve showing that the erosion resistance of annealed elemental metals increased with hardness from Zinc up to Tungsten.[3] Based upon the behavior of the elemental metals, he and many others have used as an accepted fact, even rule of thumb, that higher hardness results in greater erosion resistance. This basic premise has also been proven to be wrong in work performed by several investigators in the past three years that will be reviewed herein.

This paper is intended to bring out the body of evidence that is building toward a new way to consider erosion, one that is based on physical observation of erosion surfaces at high magnifications with great depth of field. The real mechanism of erosion is in agreement with those aspects of erosion behavior that the micro-machining mechanism could not account for as well as those that it did explain. While the new mechanism of erosion has not yet been reduced to a predictive model, it has been developed far enough to indicate which properties of ductile alloy do and do not enhance erosion resistance.

This paper should make the reader consider erosion of ductile metals in a new light. It will put in the past much of the erosion literature that has been available. It will, hopefully, intrigue engineers and scientists to pursue new directions and have new considerations come to mind when solid particle erosion of ductile metals is the concern.

THE PLATELET MECHANISM OF EROSION

A review of the evolution of the platelet mechanism of erosion of ductile metals by small solid particles will be helpful in making the transition from the micro-machining mechanism. In unpublished work conducted by the author several years ago to determine how specific steel microstructures affected erosion, an erosion weight loss technique was used that caused the basic doubt of the validity of the micro-cutting mechanism.

In order to learn more about the initiation of erosion, an incremental weight loss measurement rather than the cumulative one generally reported in the literature was used. The erosion was conducted incrementally, 60gm of particles at a time, and the weight loss caused by each 60gm increment was determined and plotted as shown in Fig. 1. It can be seen that the initial erosion rate caused by the first 60gm of SiC particles was much lower than that of subsequent 60gm batches of erodent. Also, extrapolating the curves down to 0 erosion shows that a number of grams of particles have impacted the surface before erosion losses commence. If micro-machining was the mechanism of erosion, the erosion rate of the initial, uneroded surface should be higher than subsequent incremental rates where work hardening of the surface due to the machining action would have reduced the machineability of the surface. Erosion also should have started with the first impinging particles.

It can also be seen in Fig. 1 that doubts concerning the effect of hardness and strength effects on erosion were also raised. The lowest hardness, lowest strength condition of the 1075 eutectoid steel, the spheroidized condition, had the lowest erosion rate.

The effect of work hardening of the spheroidized steel was also investigated at that early time. It was expected that as the material was worked hardened its erosion resistance would increase with the resulting hardness increase. Table 1 shows the erosion rate for the initial 60gm of erodent for 1075 steel specimens that were cold rolled to various percentage reductions prior to eroding them. The hardness doubled between the annealed steel and the 80% cold reduced steel, but the initial erosion rate, rather than decreasing with increasing hardness, increased significantly. It did not achieve the steady state incremental erosion rate, but approached it.

These two early pieces of evidence coupled with scanning electron microscope(SEM) photomicrographs showing extensive piling up of material around craters produced by single particle impacts, Fig. 2, established doubts regarding the micro-machining mechanism of erosion. These doubts were later reinforced when Fig. 3 was obtained. It shows, at low magnification, the region at the edge of the primary erosion region of 1100-0 aluminum that was eroded to the steady state condition by spherical steel shot at a relatively steep impingement angle, $\alpha=60°$. Many platelets can be seen that were made by an extrusion-forging action much the same as occurs when a soft, malleable metal like gold is beat with a ball peen hammer. Some of the platelets are bent, indicating that another impact on them could break off the bent part or even the whole platelet.

Microscopic Sequences

Combining the evidence gathered to that time, an intensive effort was made to metallographically observe the development of an eroded surface a few impacts at a time. This entailed developing a technique that would locate the same micro area in the SEM after sequential, very short erosion exposures. To do this microhardness indention markers and much patience were used. The results of this effort are reported in ref. 4.

Small particles, representative of the sizes that actually occur in erosion environments, were used so that the extent of the damage caused by individual impacts would not overwhelm the mechanism that was occurring. It was felt that the several milimeter bee-bees used by others and reported in the literature produced forces at the metal surface that were so much greater than those produced by actual eroding particles that the resulting mechanism would probably be different.

Fig. 4 shows the appearance of the surface at low magnifications at the beginning of the erosion exposure. Each 0.1gm of 600μm SiC particles consisted of 400 - 500 individual particles striking an area of approximately 1.25cm in dia. Only a few particles of the 500 struck the observed area in each incremental exposure, as can be seen by the limited amount of damage which occurred in the immediate area of the microhardness indentation markers.

Fig. 5 shows a particular area in Fig. 4 within the marked box drawn on the upper right hand picture of Fig. 4. The changes in the triangular area shown as it was struck by individual particles shows the distinct development of flattened platelets as each subsequent 0.1gm of erodent struck the eroding surface. It can be seen that after 0.4gm of erodent had been used essentially no material loss had yet occurred in the observed area. However, the tip of the traingle was knocked off, as shown in the lower right photo. This sequence accounts for the fact that there is a threshold period in erosion when no material loss occurs that is followed by a slowly increasing material loss as more particles strike the surface.

Carrying this sequential erosion experiment to steady state erosion produced the highly textured surface shown in Fig. 6. The magnified area in the figure is the region between the two sets of crossing parallel lines on the 7075 Al specimen pictured. It was eroded at an impingement angle of 30° which caused the elliptical shape. hundreds of platelets in various states of formation can be seen in the figure.

Fig. 7 shows a single region of surface at higher magnification after the specimen was impacted with an additional 2gm of particles. The platelets that were present after the first gram are shown in the upper photo. The lower photo shows the marked changes that occurred after the second gram of particles struck the surface. The platelets in the upper right part of the photo have been knocked off as has the platelet that sat astride the light line extending along the lower right side of both photos. New platelets have been extruded out from the main area of platelets in the center left side of the lower photo.

These observations formed the basis for the development of the platelet mechanism of erosion. Many additional observations were made and one is reported in ref. 4. A classic shaped distressed platelet is shown in the center of Fig. 8 surrounded by other smaller platelets. It has the appearance of a thin pancake forging with considerable edge and even some internal cracking.

All of the evidence shown thus far was developed using aluminum alloys which have FCC crystallographic structure and many active slip systems. In order to determine whether the formation of platelets is unique to metals of this type, several steel alloys were eroded and their surface microstructures were observed. All of the alloys tested, including 1020, 4340 and 304SS at various heat treat conditions, formed platelets similar in size, shape and quantity to those initially observed in aluminum alloys. Fig. 9 shows the eroded surfaces of 1020 plain carbon steel that has a BCC crystallographic structure and only a few active slip systems after erosion at impingement angles of 30° and 90°. It can be seen that the same mechanism of platelet formation occurs at both angles, thereby accounting for the significant amount of erosion that is measured at α=90°.

From the above evidence, the loss of metal from an eroding surface appears to occur by a combined extrusion-forging mechanism. Evidence has been obtained that indicates that the platelets are initially extruded from shallow craters made by the particle impact. Once formed they are forged into a distressed condition shown in Fig. 8 in which condition they are vulnerable to being knocked off the surface.

Surface Observations

Fig. 10 shows a typical crater formed on the surface of a 7075-T6 aluminum target by a single particle that was directed at a steady state erosion surface. The surface had been sputter coated with approximately 300Å of gold before the single particle test was carried out. It can be seen from the gold x-ray maps that there is a significant amount of gold in the bottom of the crater and on the extruded platelet at the lower right side of the crater. The areas that appear to be devoid of gold, the center-right side of the photo and the lower left side of the crater, are in the shadow of the extruded platelet and the steep lower left wall of the crater. The x-ray detector was located in the lower left hand corner of the photo at a relatively low angle.

The presence of gold on a crater surface that was formed by a single particle impact on a thin, 300Å thick coating of gold applied prior to the particle impact indicates that the platelet formed out of the crater, lower right in Fig. 10, was extruded out from under the gold coated surface. The actual surface was maintained by its contact with the eroding particle, resulting in the extrusion force occurring just beneath the surface.

Further evidence of extrusion being the initiating mechanism of platelet erosion was obtained in an experiment where a thin, 3μm, layer of copper was plated on a 1020 steel substrate which was subsequently eroded with a few SiC particles. Fig. 11 shows a cross section of the eroded surface area. Copper can be seen beneath the surface in the center of the photo, indicating that the steel had been extruded over it from the nearby shallow craters. A close examination of the photo shows that there is a thin layer of copper remaining on the surface of the craters. It can be seen easily in a colored photo.

Fig. 12 is a sketch of a proposed sequence of particle impacts that could cause the micrograph in Fig. 11. The lip of platelet extruded out of the crater by the first impact is identical to one shown by Gulden and Kubrych in their Fig. 11 of reference 8. Similar extruded lips are shown in several of the papers of Hutchings, including ref. 5. It can be seen that the sequence of extrusion followed by forging of the extruded material can readily account for the surface and sub-surface locations of the copper plating. The presence of the thin layer of copper over the entire surface of the craters in Fig. 11 indicates that it is extrusion that forms the lips of platelets rather than micro-machining, as machining would have removed the thin copper layer (or gold layer in Fig. 10).

Fig. 13 is a sequence of photos that shows the extrusion formation of a single platelet, its subsequent spreading by forging and, finally its removal as the result of a particle striking it. The target alloy was 7075-T6 Al. The sequence occurs in clockwise order starting from the upper left photo. The curved striations in photo 1 are covered over by the large platelet that was formed by one particle striking the right side of the metal, shown in photo 2. The platelet was extruded from the straight line, striated, shallow crater and flipped over the top of the crater formed earlier that has curved striations in its surface. The striations on the surfaces of the craters are imprints of striations that form on the fracture surfaces of the SiC particles used to erode the aluminum. Some of these striations can be seen along the sides of the SiC particles shown in Fig. 14.

The lower right photo, 3 in Fig. 13, shows how two subsequent particle strikes in the area forged the platelet out to a larger size with a sub-platelet forming at its upper left side. In the fourth photo the platelet has been knocked off the surface and the crater surface with the curved striations and a portion of the straight striations of the crater out of which the platelet was formed can be seen. The deep curved striation can be easily seen in photos 1 and 4 to identify that it is the same surface which was covered over by the platelet in photos 2 and 3.

The platelets do not adhere to the surfaces over which they are extruded. Rather they adhere to some location along the extrusion path. In the case of the platelet shown in photo 2, it is attached at the point where its right side is next to the crater from which it was extruded. In photo 3, the attachment point is now under the forged out platelet, making a mushroom type configuration. The amount of plastic deformation represented by these photos is large and could probably only have occurred on such a low elongation (11%) alloy as 7075-T6 Al if it occurred at an elevated temperature.

Surface Heating

While there is no direct evidence on any of the micrographs shown of heating of the eroding surface, considerable evidence was gathered during the course of the investigation that temperatures near the recrystallization temperature occured at the immediate eroding surface. Fig. 14 shows evidence of aluminum that has been melted and resolidified on the surface of a SiC erodent particle that was used to erode 1100-0Al. Almost all of the eroding particles that were captured and observed after the erosion process had some aluminum on them.

Considerable recent work and some older work in the literature supports the fact that adiabatic shear heating and possibly some frictional heating occurs on the surface during the erosion process. Hutchings and Winter discussed the generation of heat on an eroding surface in ref. 5. They attributed it to adiabatic shear heating when erosion lips were formed out of craters. Christman and Shewmon in ref. 6 show evidence of melting of 7075-T6 aluminum when it was eroded with 5mm steel balls which imparted very high forces and resulting deformation to localized erosion areas. Adiabatic shear bands were observed in the area where melting occurred. In ref. 7, Shewmon used the heating of the surface during erosion to calculate the effect of small particles, <100μm, causing reduced erosion rates on metals. Gulden and Kubarych saw evidence of melting on 1095 steel.[8] Brown and Edington used the low melting temperature metals gallium (mp=29°C) and indium (mp=156°C) specifically to show that erosion caused the generation of heat on the eroding surface by melting both the gallium and indium in experiments.[9]

While most recent investigators, including the ones referred to above, did not observe actual melting on most of their erosion tests, when they made the tests conditions conducive to having the heat erosion melt the target alloy, they did observe melting. Generally this required the use of low melting temperature targets or large concentration of particle kinetic energy and resultant force at the target surface by using very large particles.[6]

Literature Corroboration

The presence and documentation of platelets on eroding surfaces has been reported extensively in the recent literature. Some investigators called the platelets chips, some flakes, some lips and several called them platelets. In all instances, however, their figures showed configurations that are called platelets in this review. For example all five papers presented in the erosion session at the April, 1981 International Conference on Wear of Materials showed platelet formation on the eroded surfaces. Three of the five papers describe surface heating.[10]

In ref. 8 platelet formation is noted on 2024 Al eroded surfaces. In ref. 11, extensive platelet formation is shown. Platelet formation occurred on copper single crystals as observed by Brown and Edington in ref. 12. In reference 13, Rickerby and MacMillan carefully documented the development of platelets at the intersections of indentations caused by spheres striking the target surface. Christman and Shewmon in their work on the erosion of 7075-T6 aluminum alloy reported the generation of platelets and their removal from the surface as the erosion metal loss mechanism.[6]

Thus, a consensus has developed that erosion occurs by the generation and loss from the surface of platelet-like pieces of metal. The next step, is to combine the observations and formulate a mechanism that considers them. This has been done in ref. 4. A brief description is presented here.

Platelet Mechanism Description

Fig. 15 is a sketch of a cross section of an eroding ductile metal. The erosion heated surface, 5 - 15μm thick, consists of platelets at various stages of generation and large strain deformation. Beneath the platelet zone is a work hardened zone that developed during the early stages of the erosion exposure. This zone lies beneath the heated surface region and strain hardens as a function of the strain hardening coefficient of the target metal. Beneath the cold worked zone is base metal at whatever condition it was worked or heat treated to.

Based upon the data presented earlier it is proposed that the following sequence occurs in the erosion process. In the beginning platelets are formed, initially without loss of material (Figs. 4 and 5). Adiabatic shear heating of the immediate surface region begins to occur (ref. 5, 6, 8, 9). Beneath the immediate surface region, the mass target material forms a work hardened zone (Table 1) because the kinetic energy of the impacting particles is enough to result in considerably greater force being imparted to the metal than that required to generate platelets at the surface.

When the surface has been completely converted to platelets and craters (Fig. 6) and the work hardened zone has reached its stable hardness and thickness, steady state erosion begins (Fig. 1). The reason that the steady state erosion rate is the highest one in Fig. 1 is that the subsurface cold worked zone acts as an anvil to increase the efficiency of the impacting particles or hammer to extrude-forge platelets in the now fully heated and most deformable surface region. When the anvil is fully in place and the platelets are fully formed and heated, maximum material removal rates will occur. This cross section of material conditions will move down through the metal as erosion metal loss occurs.

To document the occurence of a heated surface area that could have reached the recrystallization temperature of the target metal and a subsurface work-hardened zone, cross sections of eroded aluminum and steel alloy specimens were prepared and microhardness tested using a very light, 5gm, load so as not to cause false readings near the surface. Fig. 16 shows the microhardness survey of an 1100-0 aluminum specimen. The lower hardness, immediate surface region can be seen, particularly for the α=30° impingement angle where erosion rates are the greatest. The hardness increase to a sub-surface work hardened zone followed by a hardness decrease to that of the base metal is also shown. Fig. 17 shows the microhardness indentations on a typical specimen. The first hardness determination was made about 5 microns in from the surface at that point. The evenness of the geometry of the indentation indicates that valid near-surface readings were obtained. In a paper by Salik and Buckley a micrograph of an eroded

6061 Al cross section is shown that labels the three regions discussed above.[10]

THE EFFECT OF MECHANICAL PROPERTIES ON THE EROSION OF DUCTILE METALS

The platelet mechanism of erosion restuctures many of the previously accepted relationships between erosion behavior and physical and mechanical properties of ductile metals. Ductility, strain hardening, malleability and thermal properties become more important, requiring that the effects of such older related properties as hardness and strength be reassessed. Several recent investigations have studied these variables. The results of investigations that varied hardness, strength, toughness, ductility and heat treatments to anneal or harden alloys will be reviewed in this section.

In work by this author several steel and aluminum alloys have been tested at various strength, hardness and ductility levels. In Fig. 1 it can be seen that a fine pearlite microstructure with a hardness of R_B 99 erodes some 40% faster at steady state erosion conditions than does the same steel in the softer, R_B 79, more ductile spheroidized condition. Fig. 18 shows the incremental erosion rate curves for 1100-0 aluminum and 7075-T6 aluminum. Both alloys formed the same type and size of platelets when eroded with SiC particles, but the erosion rates are markedly different. The 7075-T6 with a tensile strength of 76,000 PSI erodes 50% greater than the much weaker 1100-0 Al that has a tensile strength of 13,000 PSI. The 1100-0 is much more ductile than the 7075 Al, 35% compared to 11% elongation. In the case of these aluminum alloys, higher ductility results in greater erosion resistance. Higher strength and hardness results in significantly greater erosion occuring.

A series of steels was tested to determine the effects of properties on erosion behavior.[16] The effect of ductility on the erosion rates of 304SS is shown in Fig. 19. It can be seen that the less ductile, as rolled sheet has a higher erosion rate than the annealed steel.

The effect of the strain hardening coefficient is shown in Fig. 20. The amount of erodent required for the three materials tested to reach steady state erosion conditions is inversely proportional to their strain hardening coefficients. Table 2 shows this relationship. A higher strain hardening coefficient results in the formation of the sub-surface, cold worked zone anvil sooner and, hence, steady state erosion is reached with a fewer number of particles having impacted the surface.

In spite of the fact that the stainless steel and OFHC copper form a work hardened layer sooner than the 1020 steel, they erode at much lower rates at steady state conditions, see Fig. 20. This appears to relate strongly to the elongation of the alloys as shown in Table 2 and not at all to their strength. It is realized that the strain rates and actual deformation temperatures at the eroding surface are greatly different from those of the slow strain rate tensile test that is used to determine elongation. However, tensile elongation has been able to be related to erosion behavior reasonably well.

Another example of the effect of strain hardening of the sub-surface "anvil" is shown in Fig. 21 and 22. In this experiment, the impacting particle was varied and the erosion of 1020 steel determined. A weak mineral particle that fragmented on impact, apatite, and a strong particle that did not, Al_2O_3, were used with all other testing conditions being the same. Fig. 21 shows the incremental erosion curve using Al_2O_3 particles. The number of particles to reach steady state was of the order of 50gm. Fig. 22 shows the curve for the weak, apatite particle. Almost 200gm of particles were required to reach steady state erosion even though the level of that steady state erosion was only 25% as great as that which occurred when the Al_2O_3 particles were used.

It was postulated that the reason that the 1020 steel eroded with Al_2O_3 particles reached steady state erosion in less than half the particle flow it took for the apatite particle test is that the apatite fragmented into small particles when they impacted the surface. The effective size of the apatite particles after they broke up was too small with too little available kinetic energy to strain harden the sub-surface layer as effectively as the Al_2O_3 did. It thus took longer to form an "anvil" in the 1020 steel and it was not as an effective one as that formed by the Al_2O_3 particles. This effect of the breaking up of the apatite on the amount of kinetic energy that is available from its largest fragment may also relate to the particle size effect in erosion. The largest fragments of the apatite were less than the 100μm dia size below which erosion rate decreases with particle size.

One of the more surprising relationships between strength and hardness and erosion behavior is shown in Table 3 for 4340 low alloy steel. Four heat treat conditions were used to determine the effect of property levels on the erosion resistance. A change in strength from 300KSI to 100KSI UTS and hardness from Rc 60 to Rc 19 had essentially no effect on the erosion resistance. If anything, the lowest strength and hardness condition, the spheroidized condition, had the best erosion resistance. In this case the elongation variation of 3 times did not have much effect on the erosion rate either although at the minimum 8% elongation in the as-Quenched condition, the 434Q was in a ductile condition. It can also be seen in Table 2 that fracture toughness and Charpy impact strength also had no effect on the erosion rates.

Table 4 shows the effect of testing above and below the ductile-brittle transition (DBTT) of 1020 steel (-18°C) on its erosion resistance. The low temperature test was run by strapping the specimen to a piece of dry ice (mp -78°C) before inserting it in the erosion tester. It can be seen that the erosion rate goes up considerably when the steel is tested below its DBTT where it only has 1 - 5% elongation, compared to 25% in its above DBTT, more ductile condition.

There is considerable evidence in the recent literature to support the idea that higher strength and hardness do not generally result in greater erosion resistance within families of alloys. Gulden, in a continuing research program, found that there was no difference in the erosion rates of 1095 steel specimens tested over a tensile strength range of 3 times.[7, 18] These results compare favorable with those determined in the 4340 tests reported in Table 3. Both test series were tested at a 30° impingement angle. However, at a 90° impingement angle she found that the lowest strength and hardness heat treat conditions (Rc 30) resulted in a considerably lower erosion rate compared to the highest hardness (Rc 66) condition. This further substantiates the beneficial effect of greater ductility on erosion resistance.

In ref. 8 Gulden reported that 2024-T6 aluminum eroded considerably more than the weaker but more ductile 2024-0 aluminum. This compares with the results shown in Fig. 18 comparing 7075-T6 with 1100-0 Aluminum. In further tests on 1095 steel she measured erosion rates that were 2½ times higher for the Rc 66 full hard condition compared to the Rc 20 annealed condition. However, in erosion tests of binary Fe-Cr alloys that were hardened by solid solution strengthening rather than strained lattice hardening as occurs in the 1095 steel, she observed that erosion resistance did vary directly with hardness. This behavior relates to Finnie's curve in ref. 3 for elemental metals where hardness directly related to erosion resistance.

In reference 15 it was reported that there was no correlation between the hardness as varied by heat treatment and the erosion behavior of 6061 aluminum and 1045 steel. In these alloys, the lattice is strained by precipitation hardening (6061Al) and martensite formation (1045 steel) to achieve the higher hardness with attendant decrease in ductility. In references 7 and 14 Shewmon reported that higher hardness or fracture toughness did not enhance erosion resistance.

Thus a body of evidence is growing that relates higher erosion resistance to the increased ductility of the metal rather than to higher strength and hardness. This behavior correlates well with the platelet mechanism of erosion of ductile metals. The ability to plastically deform to absorb the force from the kinetic energy of the impacting particles so that the local fracture stress of the metal platelets that are formed is not exceeded results in lower erosion rates. However, there is a limit to the effect ductility has on increasing the erosion resistance of a ductile metal at the expense of strength. In ref. 16, Foley and Levy defined that tradeoff for 1020 steel. A point is reached where the strength of an alloy has been reduced to such a low level that localized fracture stresses can be exceeded and erosion rates begin to increase with further strength reductions even though the ductility is still increasing.

THE DELAMINATION WEAR THEORY IN EROSION

An additional mechanism of erosion to the platelet mechanism by extrusion-forging has been observed. It primarily occurs in multiphase alloys where at least one phase consists of isolated hard particles in a softer matrix of the major phase. This type of erosion also produces platelets that are knocked off of the surface by succeeding particles. It occurs in combination with the platelet mechanism of erosion described earlier. The mechanism is very similar to the delamination theory of wear developed by Suh, initially for sliding type wear.[18] Work at this laboratory by Jahanmir, who aided Suh in development of the delamination wear theory, extended that theory to solid particle impingment erosion.[19]

The effort to adapt the sliding wear mechanism to erosion was based on the structure of an eroded 1075 spheroidized steel cross section seen in Fig. 23. It shows a region some 7 to 20μm below the surface that is heavily voided and cracked. The same type of sub-surface void and cracked zone is observed in sliding type wear; the difference is in the layer of metal above the delaminated zone. In sliding type wear this zone is heavily deformed material, thought to be a dislocation sink area by Suh. As can be seen in Fig. 23, in erosion, this area consists of essentially undeformed metal until the immediate surface is reached where a surface formed platelet is seen. Branches from the cracked zone periodically reach the surface, probably due to the surface forces of the extrusion-forging mechanism of platelet formation, and larger, thicker platelets are removed from the surface.

Jahanmir, starting with the stress distribution model that he developed with Suh for sliding type wear, modified it to describe the stress and strain distribution beneath an impacting particle.[19] Using the criteria for void formation in the original delamination theory, which is twice the shear yield stress, Jahanmir plotted those regions under an impacting erosive particle where the shear stress equalled or exceeded the critical shear stress for void formation and subsequent crack propagation from the void. The critical stress is that which can exceed the cohesive bond between the hard, 2nd phase particle and the soft matrix.

The resulting plots as a function of the impingement angle of the particle, from $\alpha=5°$ to $\alpha=40°$ are shown in Fig. 24. If one combines the severity of the stress levels and the extent of the region under the impacting particle that exceeds 2 times γ_{rr}, it can be seen that the impingement angle where both considerations peak is at about 20° angle where maximum erosion is measured. Thus, there is some validity to the adaption of the delamination theory of wear to the erosion process.

There are several examples of sub-surface void formation and cracking in the recent literature. In ref. 8, Gulden and Kubraych observed it when testing 2024 Al. Brown and Edington observed it in erosion test of copper and iron in ref. 11 and 12.

ELEVATED TEMPERATURE EROSION

The effect of increasing the bulk temperature of an eroding alloy on its erosion rates is a variable one. The erosion rate of different materials can increase or decrease with increasing temperature up to an intermediate elevated temperature with respect to its melting temperature. Above this temperature all metals undergo a relatively rapid increase in erosion rate with increasing temperature. This behavior is also sensitive to impingement angle. The decrease in the erosion rate of alloys with temperature generally occurs at steep angles while the rate increases with temperature at shallow angles.

Erosion Rates

Fig. 25 plots the erosion rate of 310SS at temperatures up to 900°C. Four runs were made at the same conditions with a different specimen being used for each data point. It can be seen that at the 30° impingement angle, the erosion rate remained near constant to about 400°C and then rapidly increased at higher temperatures. At 90° impingement angle, the erosion rate decreased with increasing temperature to about the same 400°C and subsequently increased with increasing test temperature.

The almost flat curve to 400°C followed by a rapid increasing rate of erosion at α=30° was also observed by Keshevan at Union Carbide for mild steel.[26] The same pattern of increasing erosion rate with temperature at α=30° and decreasing rate at α=90° was also observed for stainless steel by Gat and Tabakoff in ref. 21. For other alloys reported in ref. 21, the erosion rate increased with increasing test temperature at all impingement angles.

Fig. 26 shows a curve of erosion rate v.s. impingement angle for 1100-O Al eroded with 250μm SiC particles at several homologous temperatures. The erosion rate generally decreased with increasing homologous temperature, especially at impingement angles between α=30° and 80°. At α=90° for the lower three test temperatures, there was no difference in the erosion rate. At the highest test temperature, near the melting temperature of the aluminum, the

the rate of erosion was higher than the other 3 test temperatures at all angles greater than $\alpha=30°$.

Microstructures

Microscopic observations of the surface and cross section of the 310SS whose erosion rates were plotted in Fig. 25 showed that the platelet mechanism of erosion was the active mechanism at all temperatures and all impingement angles. Fig. 27 shows that the nature and size of the craters and platelets was the same for both $\alpha=30°$ and $\alpha=90°$ angles. As the test temperature was increased from 25°C to 775°C, there was a small but discernable increase in the size of the shallow craters produced.

Fig. 28 shows a cross section of the eroded surface at two magnifications. Several platelets can be seen still attached to the surface in the upper photo. Extensive cracking in the attachment stem of one of the platelets (the one between the two scratch marks) can be seen in the lower photo. This platelet is very near to being removed, probably by only one or two more particle impacts.

Fig. 29 is a cross section of a 1020 steel cylinderical test specimen that was tested in a combined erosion-corrosion enviornment as a probe inserted into a propane burner tube perpendicular to the wall. The test was conducted in the Sandia National Combustion Research Laboratory exhaust gas test system. Flyash of 5μm average particle size was injected into the burner gas flow upstream of the specimen. The test was conducted for 55 minutes at a velocity of 17mps. The particle flow was stopped several minutes before the corrosive gas flow was stopped. This allowed an iron oxide scale (dark gray) to build up around the platelets that had been formed on the surface, thereby protecting them during the subsequent specimen cutting and polishing operations.

A major platelet can been seen in the center of the figure with several smaller ones on either side of the largest one. The unique protection provided by the iron oxide that formed around the platelets after the flyash flow was cut off made it possible to obtain and excellent cross section of the type of thin platelets that form on ductile metals during erosion.

<u>Erosion Mechanism</u>

The different erosion behavior of various alloys at various test temperatures, particularly the effect of impingement angles and which of the alloys tested had decreasing erosion rates, can be explained in good part by the platelet mechanism of erosion. Since the basic mechanism of erosion causes heating of the eroding surface to or near to its crystallization temperature, the bulk test temperature does not directly effect the platelet forming and removal mechanism. However, the bulk temperature has an indirect effect by modifying the development and ultimate hardness of the sub-surface, cold worked layer. This, in turn affects the efficieny of platelet formation and removal. The harder and more developed the cold worked zone is, the better anvil it becomes and the easier it is for the kinetic energy of the impacting particles to be transformed into extrusion and forging forces in the immediate surface region.

As the temperature of the bulk metal is increased, the strain hardening coefficient decreases, especially for FCC metals and a poorer anvil is developed. This is particularly important for erosion at steep angles as will be discussed below. Thus, for FCC alloys, the erosion rate decreases with increasing temperature, as is shown in Fig. 25 for the steep, α=90°, impingement angle. The strain hardening rate of BCC and HCP metals are less dependent on temperature. Above a certain temperature, which varies with the alloy, the decreased efficiency of the impacting particles to form platelets is offset by the marked decrease in the overall strength of the alloy and the erosion rate starts to increase with increasing test temperature. How the effects of strain hardening and strength reduction offset one another to result in increasing or decreasing the erosion rates of various alloys must be determined for individual alloys.

The impingement angle dependence of the erosion rates of alloys with test temperature can also be explained by the platelet mechanism of erosion.

At steep angles, the formation of platelets by extrusion of metal horizontally out of shallow craters and their subsequent forging into a highly distressed condition is more directly dependent on the presence of the sub-surface cold worked zone than it is at shallow angles. At shallow impingement angles the horizontal oriented extrusion of platelets is aided by the horizontal force component that is due to the trajectory of the particles. Therefore, the hardness of the anvil is less important to the efficiency of platelet formation at shallow angles. As shown in Fig. 25, this results in greater material loss at $\alpha=30°$ at elevated temperatures and no initial decrease in erosion rate with temperature, even for the FCC austenitic stainless steel tested. At $\alpha=90°$, the less well formed sub-surface anvil at lower elevated temperatures results in a lower erosion rate.

CONCLUSIONS

1. The mechanism of erosion of ductile metal alloys by small impacting solid particles occurs by the extrusion and forging of thin platelets which are subsequently knocked off the surface.

2. The ductility of metal alloys as measured by their tensile elongation correlates most closely of all mechanical properties investigated with erosion resistance.

3. Strength and hardness of ductile metals, except for solid solution strengthed alloys, do not directly relate to the erosion resistance of the alloys.

4. A sub-surface, cold worked zone which acts as an anvil to increase the erosion efficiency of the impacting particles is developed by plastic deformation resulting from the force applied by impacting particles.

5. The strain hardening coefficient of alloys relates to how soon the alloy reaches a steady state erosion condition, i.e., the development of its sub-surface cold worked zone, but not to the magnitude of the steady state erosion rate.

6. The eroding surface of a ductile metal is heated by the erosion process to temperatures in the annealing range of the alloy.

7. In some alloys, particularly those with small, hard, second phase particles in a softer, more ductile matrix, a sub-surface delamination mechanism of erosion occurs in addition to the surface platelet mechanism.

8. Erosion rates of steels start to increase rapidly with increasing test temperature at about 400°C. Prior to reaching that temperature the rates either do not change measureably or actually decrease with increasing temperature.

ACKNOWLEDGMENT

This work is supported by the Technical Coordination Staff of the Office of Fossil Energy of the U.S. Department of Energy under Contract Number DE-AC03-76SF00098 through the Fossil Energy Materials Program, Oak Ridge National Laboratory, Oak Ridge, TN.

REFERENCES

1. Finnie, I.; "The Mechanism of Erosion of Ductile Metals"; Proceedings Third U.S. National Congress of Applied Mechanics, ASME: New York, pp. 527 - 532; 1958

2. Finnie, I. and McFadden D.; "On the Velocity Dependence of the Erosion of Ductile Metals by Solid Particles at Low Angles of Incidence"; Wear 48 No. 1, pp. 181 - 190; May 1978

3. Finnie, I. Wolak, J., Kabil, Y.; "Erosion of Metals by Solid Particles"; Journal of Materials, 2, pp. 682 - 700; ASME: 1967

4. Bellman, R. Jr. and Levy, A.V.; "Erosion Mechanism in Ductile Metals"; Wear 70 No. 1, pp. 1 - 28; July, 1981

5. Winter, R. and Hutchings, I.; "The Role of Adiabatic Shear in Solid Particle Erosion"; Wear 34, pp. 141 - 148; 1975

6. Christman, T. and Shewmon, P.; "Adiabatic Shear Localization and Erosion of Strong Aluminum Alloys"; Wear 54 No. 1, pp. 141 - 146; May 1979

7. Shewmon, P.; "Particle Size Threshold in the Erosion of Metals"; Wear 68 No.2, pp. 253 - 258; May 1981

8. Gulden, M.E. and Kubarych, K.G.; "Erosion Mechanisms of Metals"; Report SR81-R-4526-02, Solar Turbines, Inc. San Diego, California; November 30, 1982

9. Brown, R. and Edington, J.; "The Melting of Metal Targets During Erosion by Hard Particles"; Wear 71 No. 1, pp. 113 - 118; September 1981

10. Proceedings of the International Conference on Wear of Materials"; ASME; San Francisco, California; March 30 - April 1, 1981

11. Brown, R., Jun, E., and Edington, J.; "Mechanisms of Solid Particle Erosive Wear for 90° Impact on Copper and Iron"; Wear 74 No. 1, pp. 143 - 156; December 1982

12. Brown, R. and Edington, J.; "Erosion of Copper Single Crystals Under Conditions of 90° Impact"; Wear 69 No.3, pp. 369 - 382; July 1981

13. Rickerby, D. and MacMillan, N.; "The Erosion of Aluminum by Solid Particle Impingement at Normal Incidence"; Wear 60 No.2, pp. 369 - 382; May 1980

14. Christman, T. and Shewmon, P; "Erosion of A Strong Aluminum Alloy"; Wear 52 No. 1, pp. 57 - 70; January 1979

15. Salik, J. and Buckley, D.; "Effect of Mechanical Surface and Heat Treatments on Erosion Resistance"; Proceedings of the International Conference on Wear of Materials; ASME: San Francisco, California; March 30 - April 1, 1981

16. Foley, T. and Levy, A.; "The Effect of Heat Treatment on the Erosion Behavior of Steels"; LBL Report No. 13745; Lawrence Berkeley Laboratory, University of California, Berkeley, California; April, 1982

17. Gulden, ME.: "Influence of Brittle to Ductile Transition on Solid Particle Erosion Behavior"; Proceedings of the Fifth International Conference on Erosion by Liquid and Solid Impact; Cambridge, England; September 1979

18. Suh, N.; "Special Issue: Delamination Wear and Ferrography"; Wear 44 No. 1, pp. 1 - 162; August 1977

19. Jahanmir, S.; "The Mechanics of Subsurface damage in Solid Particle Erosion"; Wear 61 No. 2, pp. 309 - 324; June 1980

20. Tabakoff, W.; "Investigation of Metals Erosion in High Temperature Particulate Flows"; Proceedings of Conferences on Corrosion/Erosion of Coal Conversion System Materials; NACE; Berkeley, California; January, 1979

21. Gat, N. and Tabakoff, W.; "Effects of Temperature on the Behavior of Metals under Erosion by Particulate Matter"; Journal of Testing and Evaluation: ASTM: 8 No. 4, pp 177 - 186; July 1980

22. Schaefer, A., et al; "A Program to Discover Materials Suitable for Service Under Hostile Conditions Obtaining in Equipment for the Gasification of Coal and other Solid Fuels"; The Metals Properties Council; 1981 Annual Report

23. Barkalow, R., Goebel., J. Pettit, F.; "Materials Problems in Fluidized Bed Combustion Systems - High Temperature Erosion-Corrosion by High Velocity (200 mps) Particles"; EPRI CS-1448; May 1980

24. Hanson, J., Kelly, J., Wood, F.; "Erosion Testing of Potential Valve Materials for Coal Gasification Systems;" U.S. Bureau of Mines Report of Investigations 8335; 1979

25. Wright, J. and Herchenroeder, R.; "High Temperature Erosion-Corrosion of Alloys"; EPRI CS-1454; July 1980

26. Keshevan, M.K.; Private communication; Union Carbide Corporation Coatings Service Department, Indianapolis, Ind. 46224

TABLE 1

EFFECT OF COLD WORK ON THE INITIAL EROSION RATE
OF SPHERODIZED 1075 STEEL

% Cold rolled	Hardness, VHN 1000gm. load	Initial erosion rate from 60gm. of SiC particles in g/g
0	152	0.98×10^{-4}
20	242	1.03
40	262	1.49
60	288	1.66
80	316	1.72
		steady state erosion rate 2.2

TABLE 2

STRAIN HARDENING EFFECT ON STEADY STATE EROSION

Metal	UTS* in KSI	ELONG.* in 2 "	HARDNESS* RB	STRAIN° HARDENING COEFF.,	APPROX. WEIGHT OF PARTICLES TO REACH STEADY STATE EROSION IN GRAMS
1020 Steel	65	36	79	0.1	200
OFHC Copper	32	55	—	0.3	100
304SS	84	55	80	0.5	60

* ASM metal process data book 1981

° R. Hertzberg; "Deformation of Engineering Materials"; Wiley, New York, 1976

TABLE 3

EFFECT OF DUCTILITY, STRENGTH, TOUGHNESS, HARDNESS ON EROSION BEHAVIOR OF 4340 STEEL

HEAT TREAT CONDITION	UTS in KSI	HARDNESS Rc	K_{1c} in KSI $\sqrt{in}$	ELONG. in %	CHARPY IMPACT STRENGTH in ft lbs	STEADY STATE EROSION in mg*
as-quenched	307	60	34	8	10	1.03
200°C	273	53	58	11	16	0.97
500°C	182	39	62	14	12	0.97
spheroidize anneal	∿100	∿19		∿25		0.90

*Statistical average of weight loss per 30gm load of 140μm Al_2O_3 particles at steady state erosion

α = 30 V = 30mps

T = 25°C

TABLE 4

EFFECT OF DBTT OF 1020 CARBON STEEL ON EROSION

TEST TEMP.	ELONG. in %	STEADY STATE EROSION* in mg
25°C	25	0.25
∿-78°C	1-5	0.82

(DBTT = -18°C)

Statistical average of incremental weight loss per 30gm load of 140μm Al_2O_3 at steady state

α = 90° V = 30 mps

T = 25°C

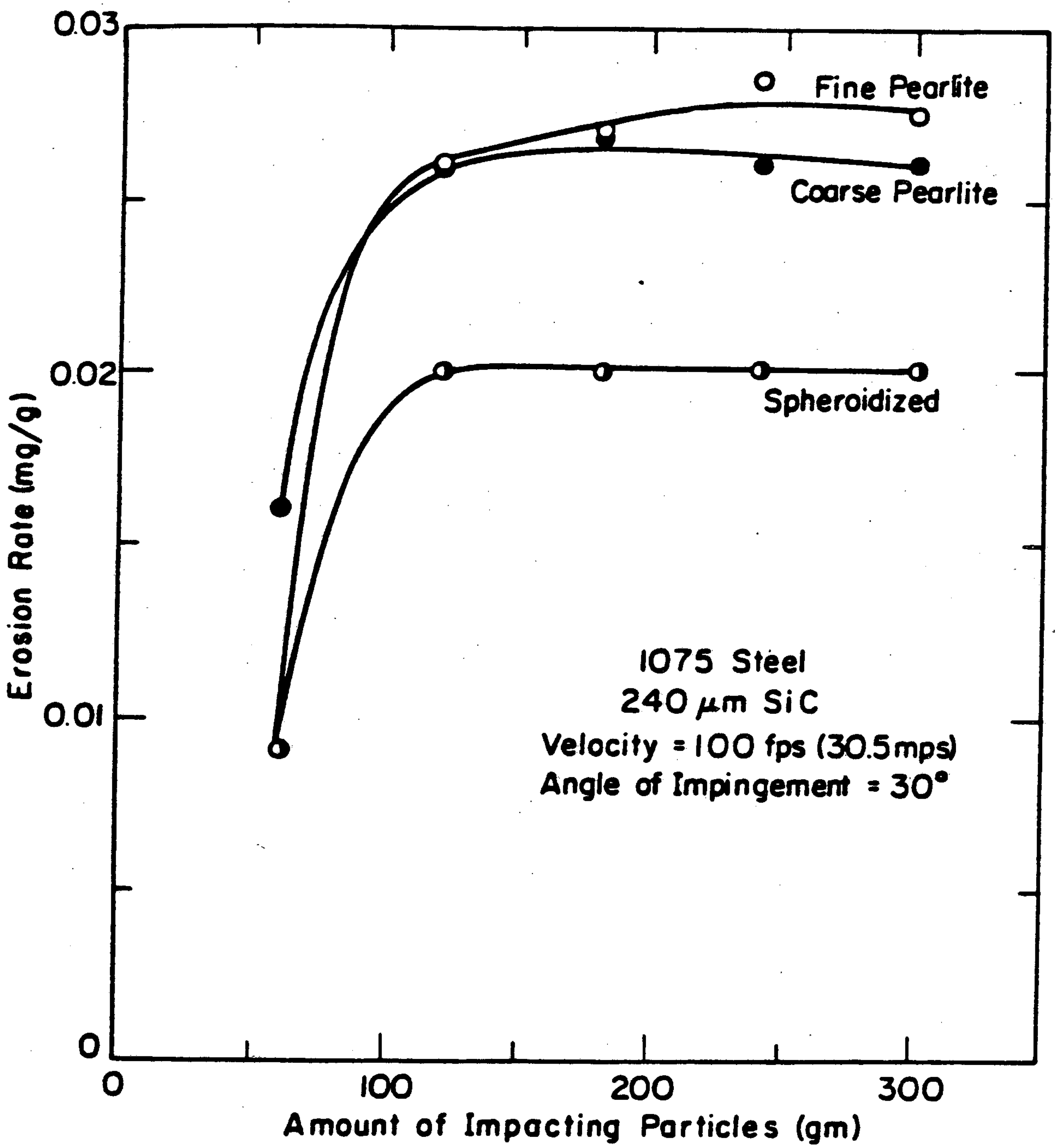

Fig. 1 Incremental erosion of 1075 steel to steady state rate XBL775-5486

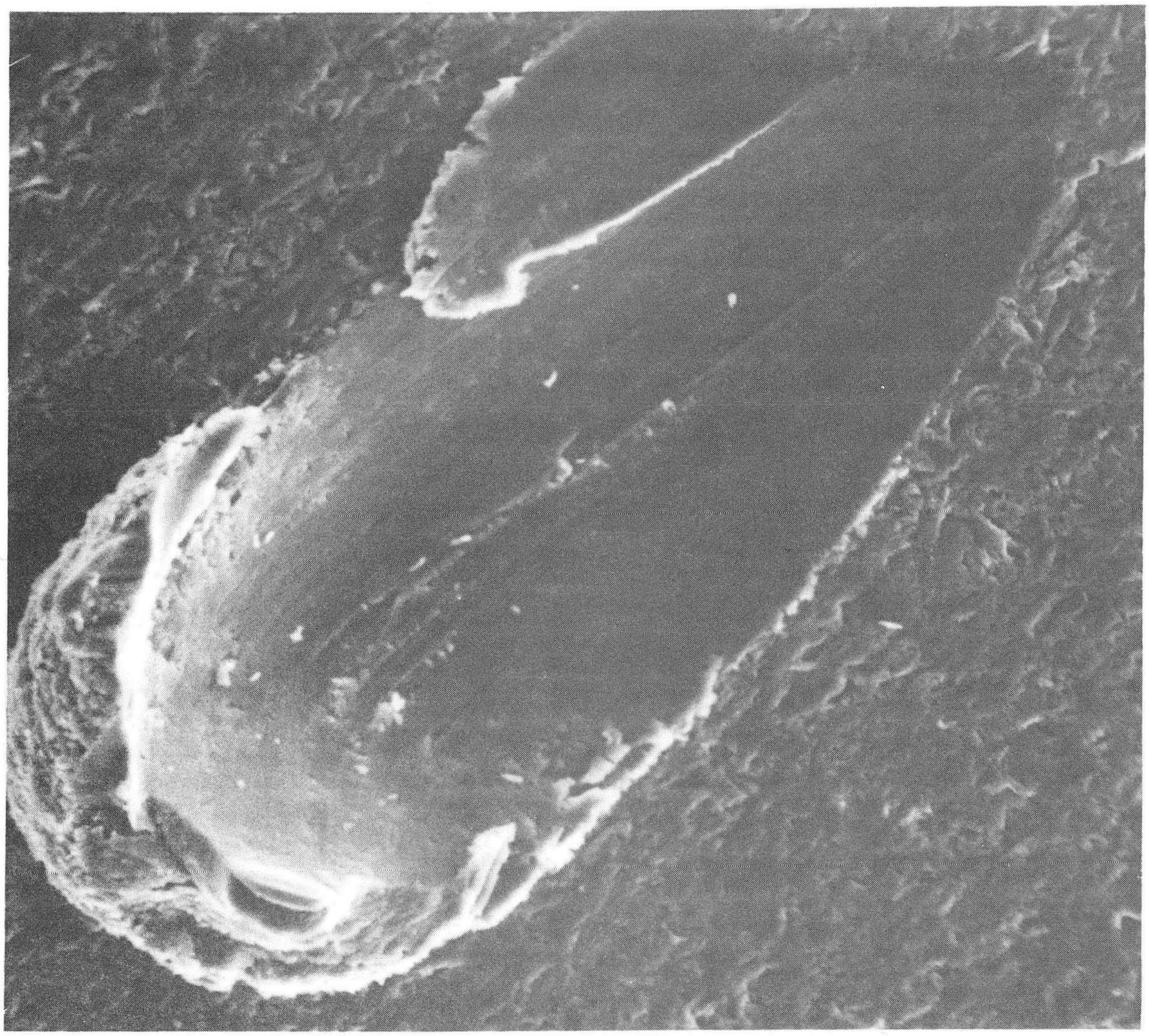

10μm

Fig.2 Single particle impact crater on 1100-0 Al

XBB7512-8747

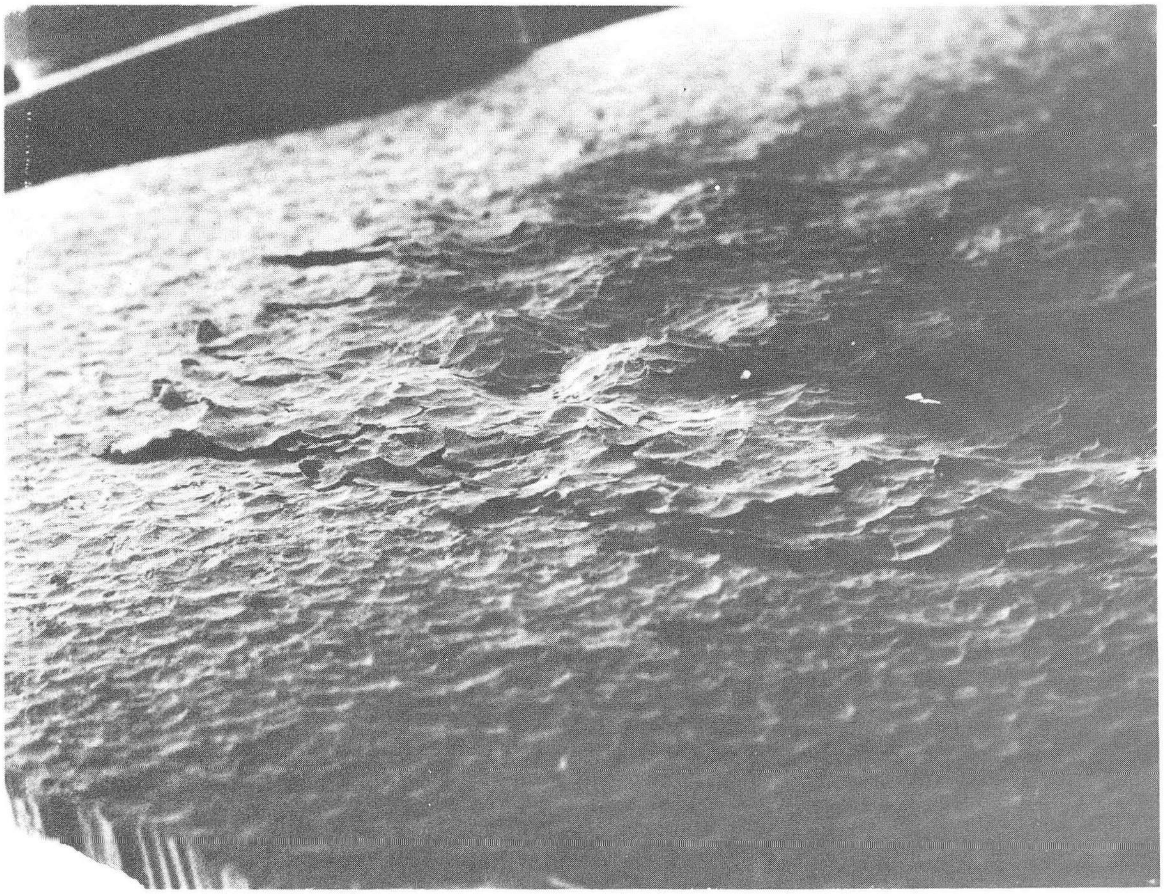

Al 1100-0 eroded with 700 μm dia. steel spherical shot. Velocity = 62 mps (200 fps) α = 60° 20X

Fig. 3 Platelets at edge of primary erosion zone of 1100-0 Al

XBB780-13772

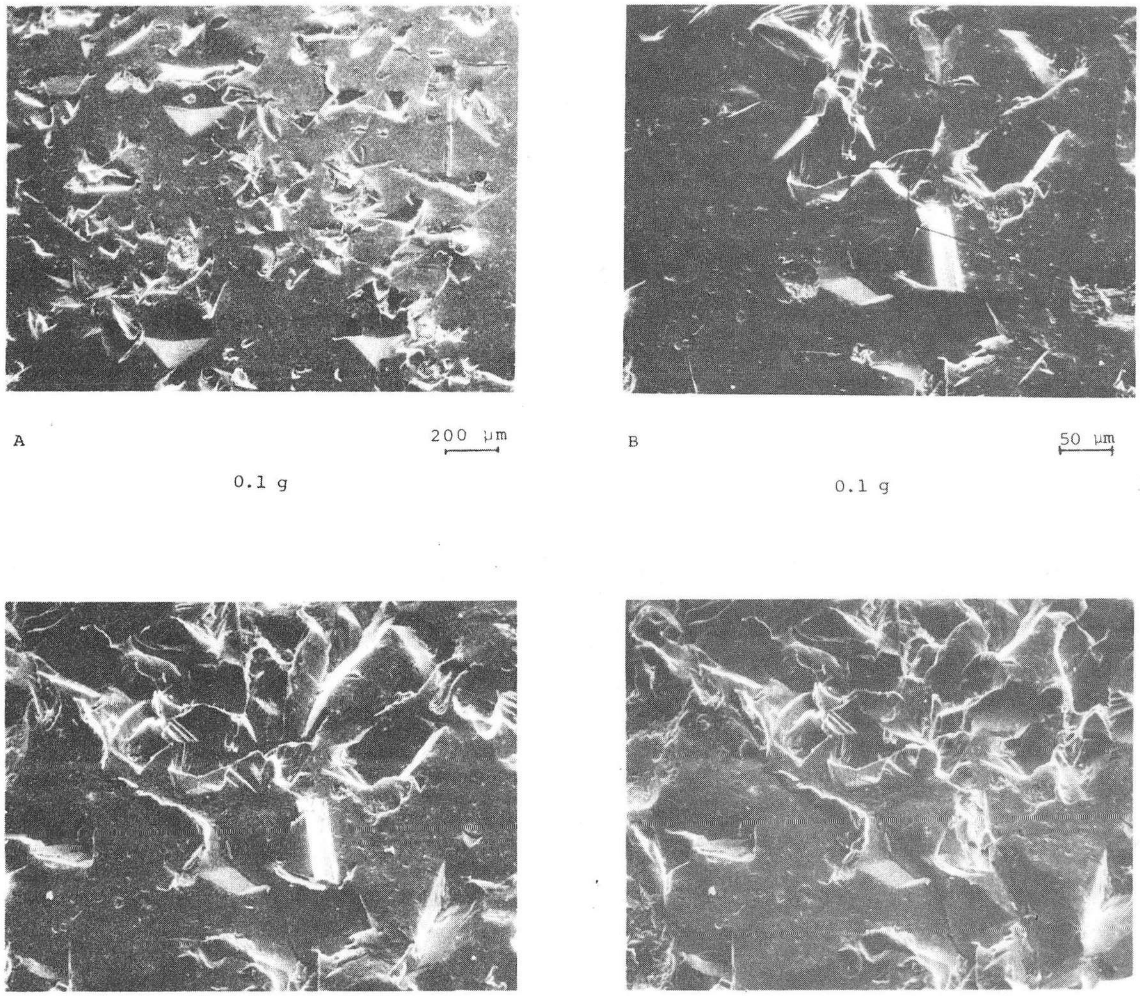

A 200 μm 0.1 g

B 50 μm 0.1 g

C 0.3 g 50 μm

D 0.4 g 50 μm

Fig. 4 Appearance of surface of 1100-0 Al early in erosion process

XBB7910-13298A

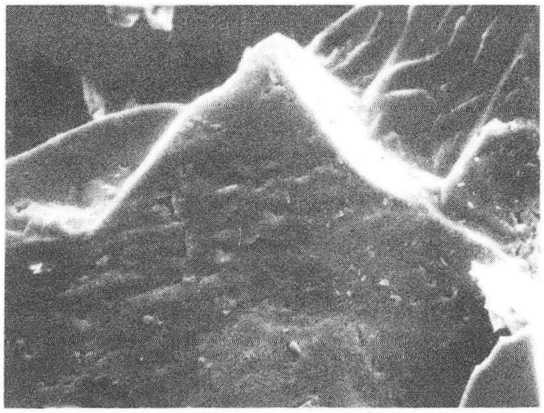

A 10 μm

0.1 g

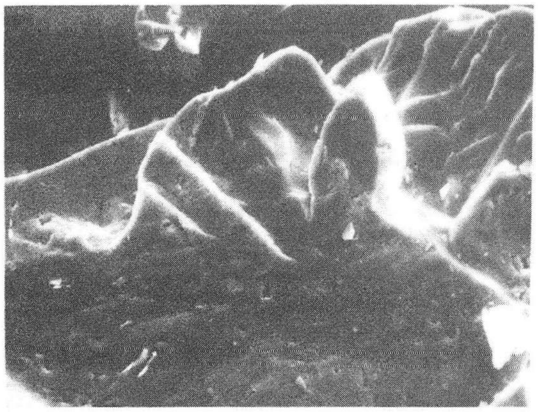

C 10 μm

0.3 g

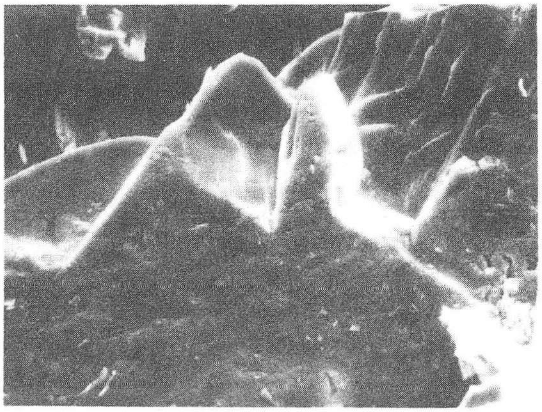

B 10 μm

0.2 g

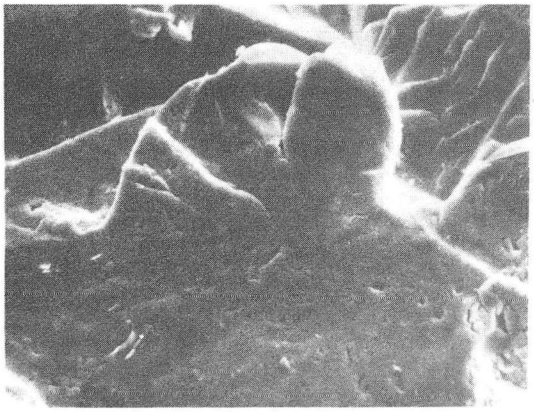

D 10 μm

0.4 g

Fig. 5 Higher magnification views of eroded area of 1100-0 Al in Fig. 4B

XBB7910-13300A

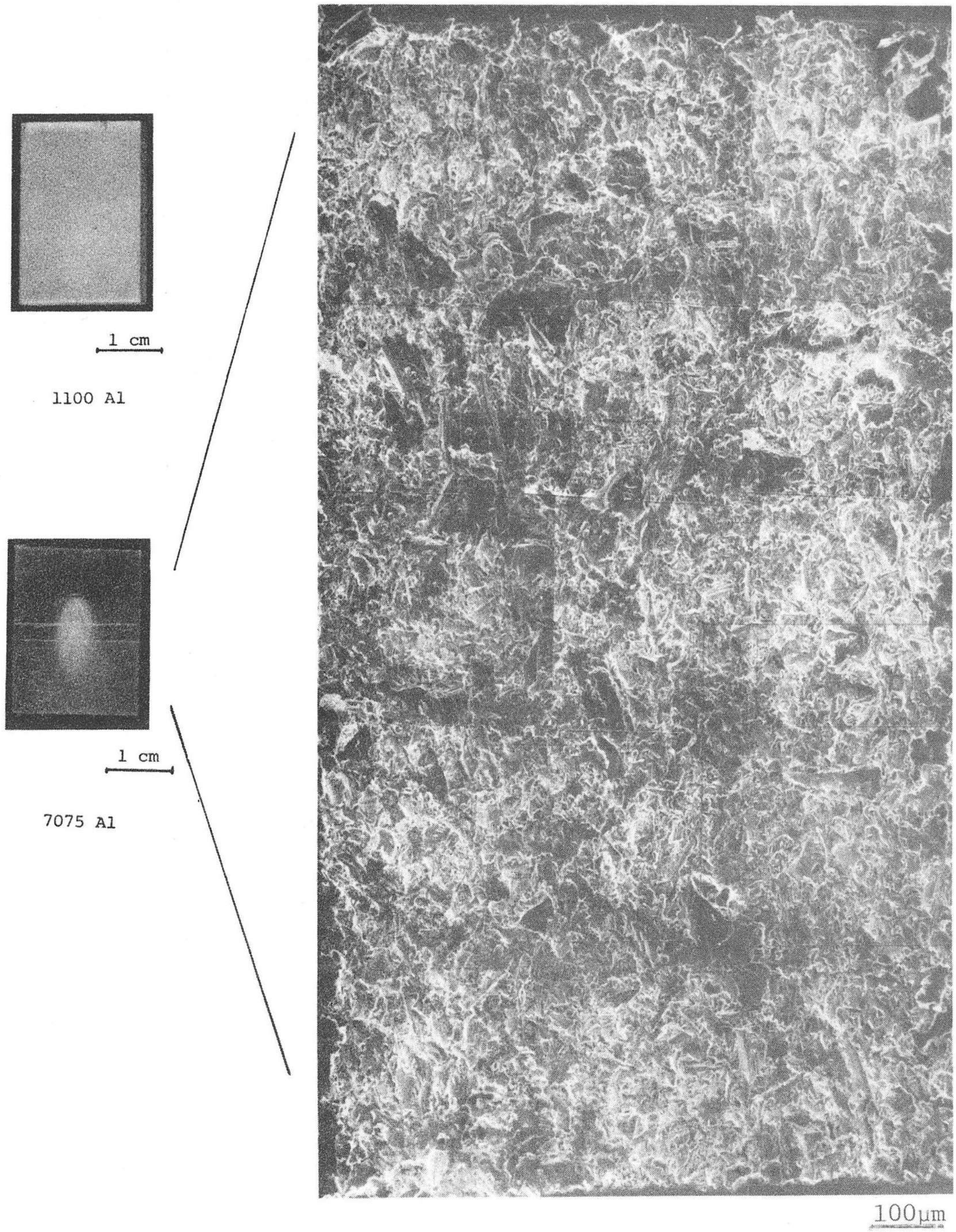

Fig. 6 Steady state eroded surface of 7075-T6 Al

XBB806-7868

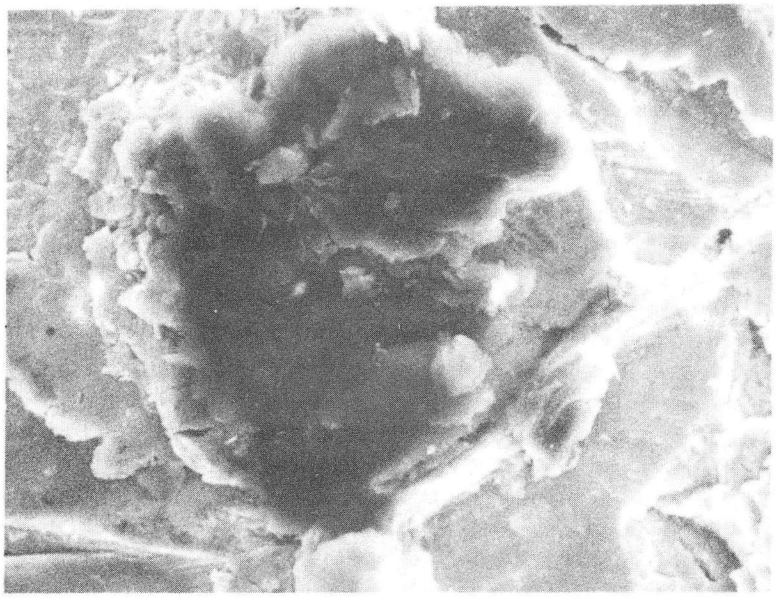

A

10 μm

1g

IMPACT DIRECTION

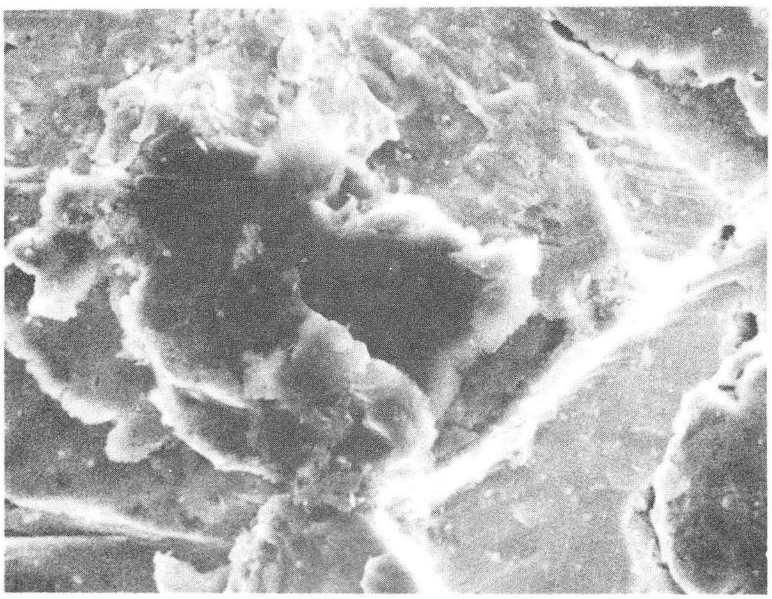

B

10 μm

2g

XBB7910-13307A

Fig. 7 Development and loss of platelets on eroded 7075-T6 Al

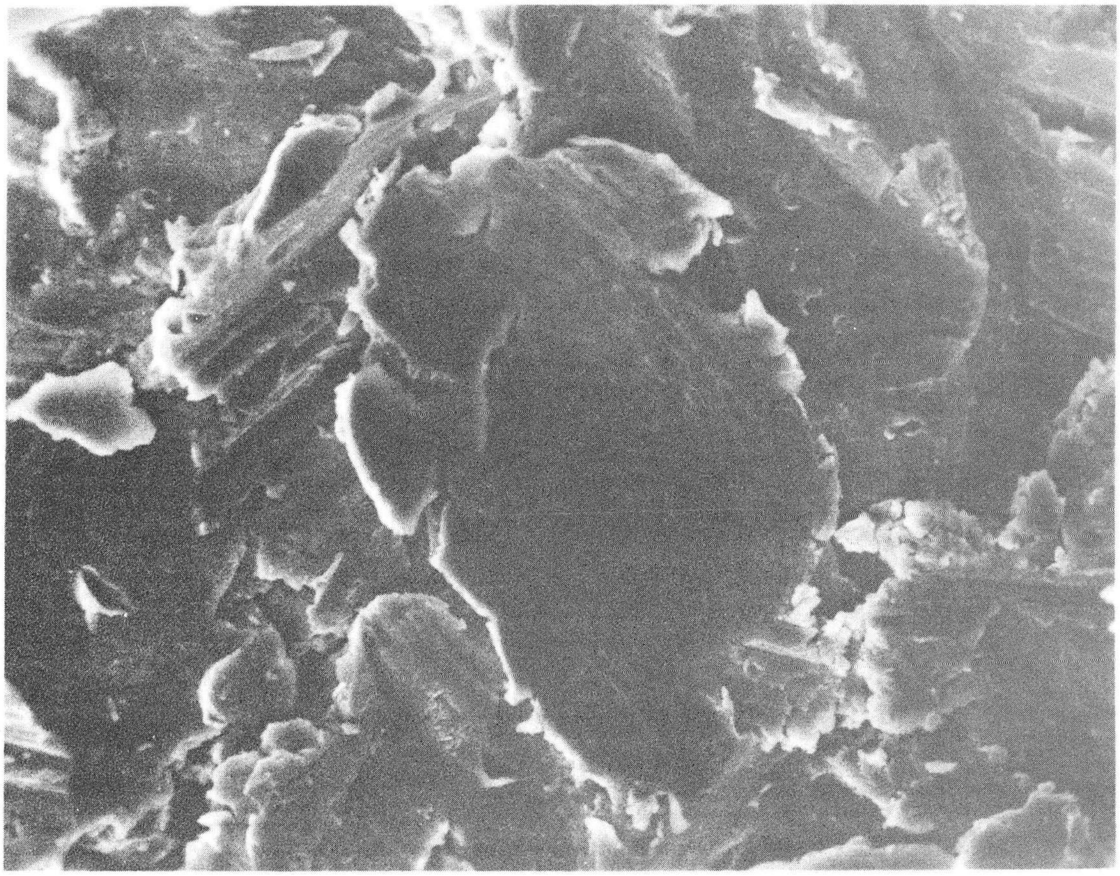

Fig. 8 Erosion platelet on 7075-T6 Al

XBB806-7866

SPHEROIDIZED AISI 1020 STEEL

30° 90°

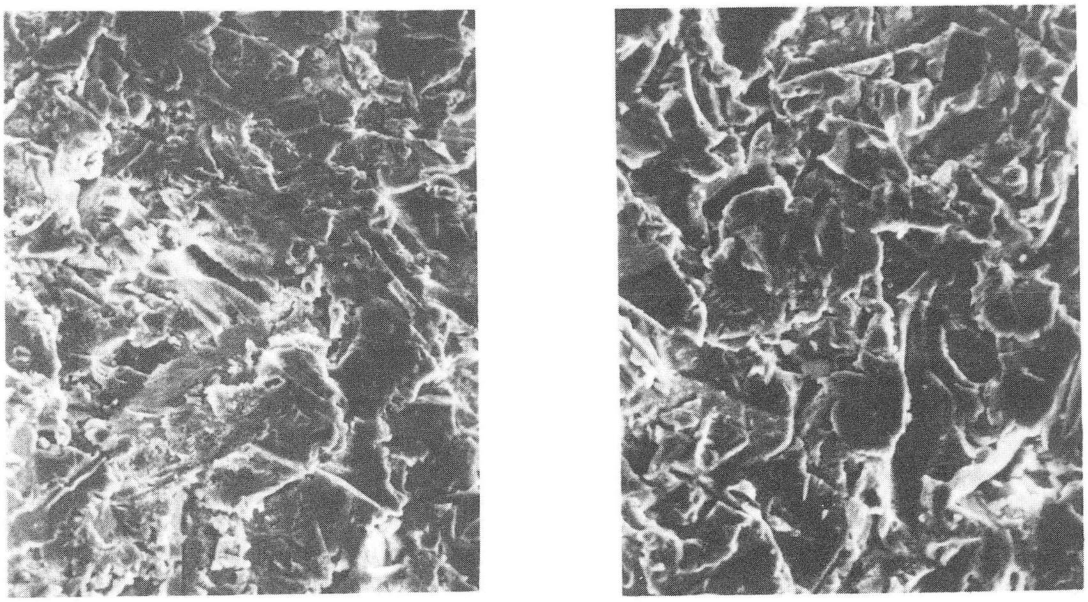

5um 5um

$V = 60\ ms^{-1}$ (200 fps)

140 um Al_2O_3

Fig. 9 Eroded surface of spheroidized 1020 steel at $\alpha = 30°$ and 90°

XBB825-4372

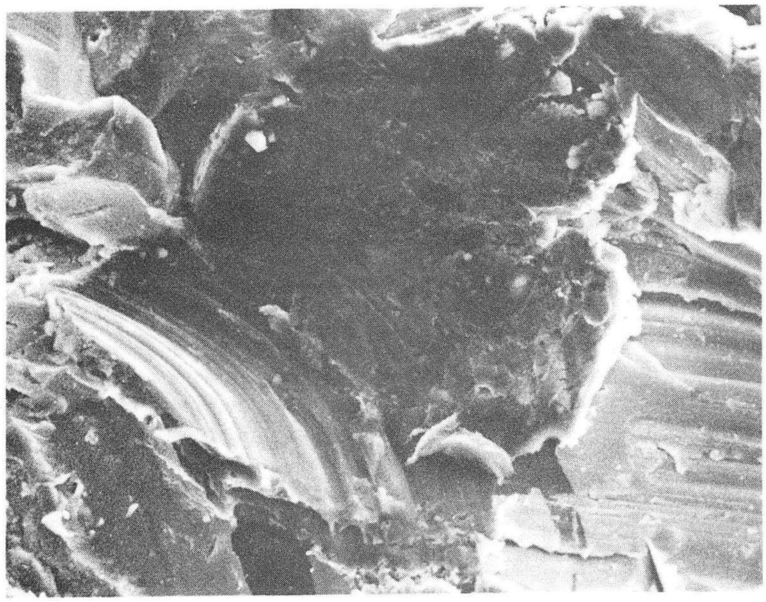

10 μm

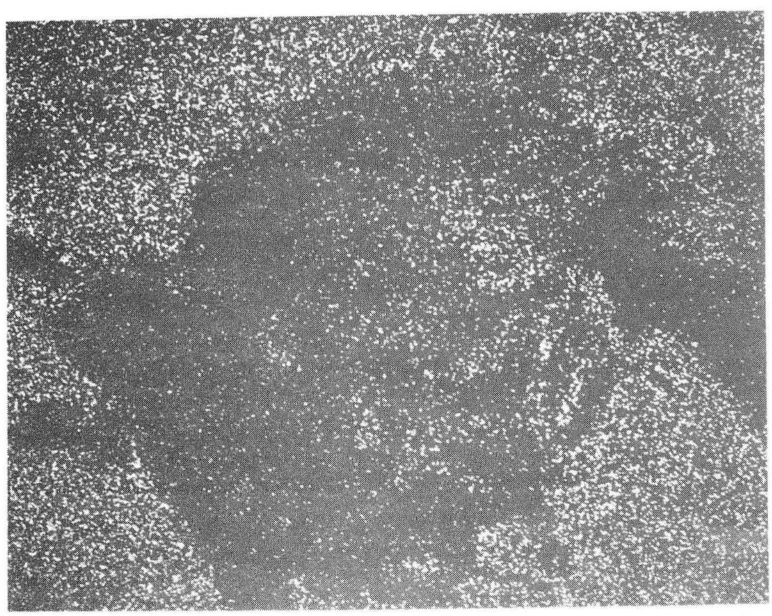

GOLD MAP

Fig. 10 Crater with residual gold over extruded surface

XBB7910-13303A

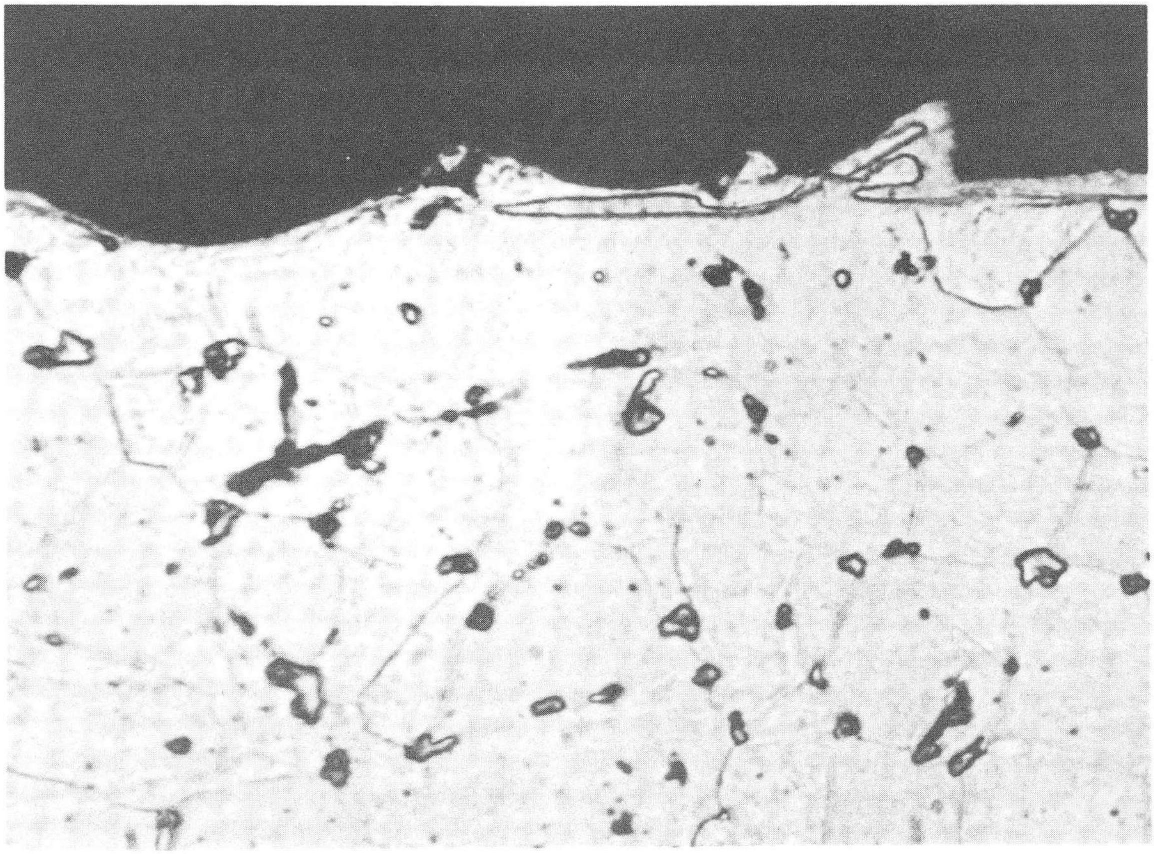

Fig. 11 Cross section of eroded surface area of copper plated steel

CBB790-12833A

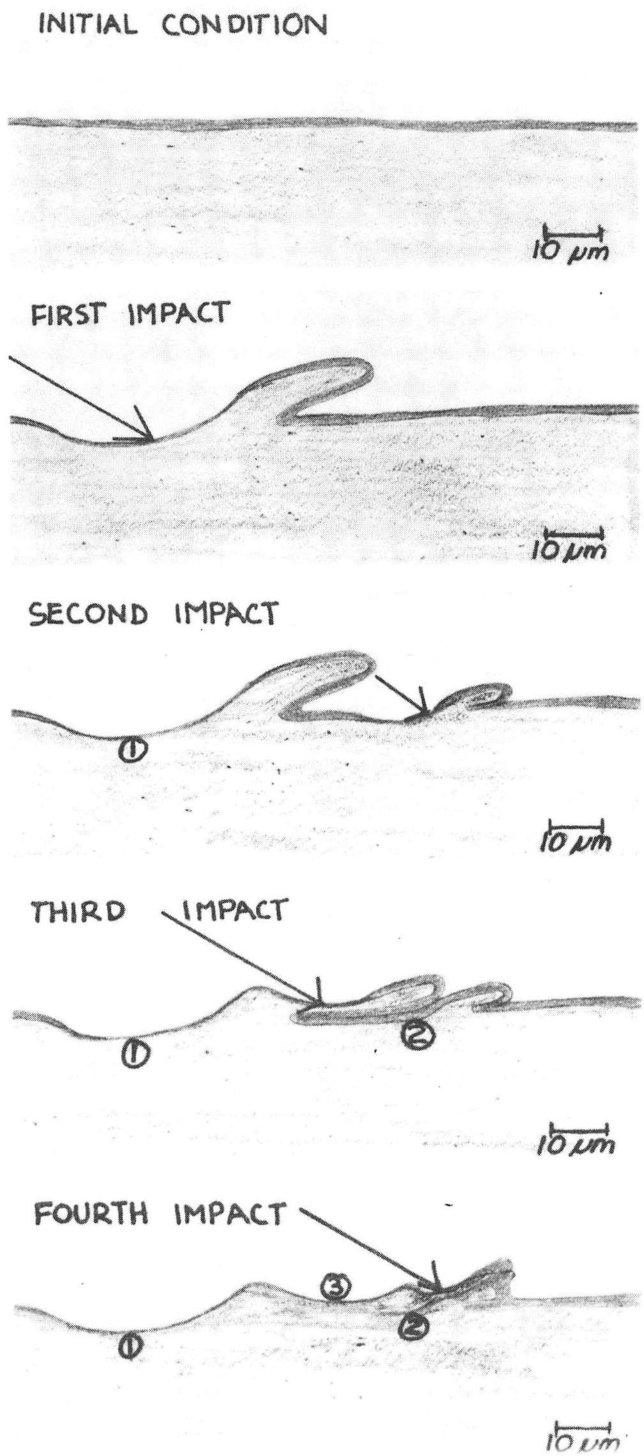

Fig. 12 Proposed sequence of erosion of copper plated steel specimen

CBB823-1717

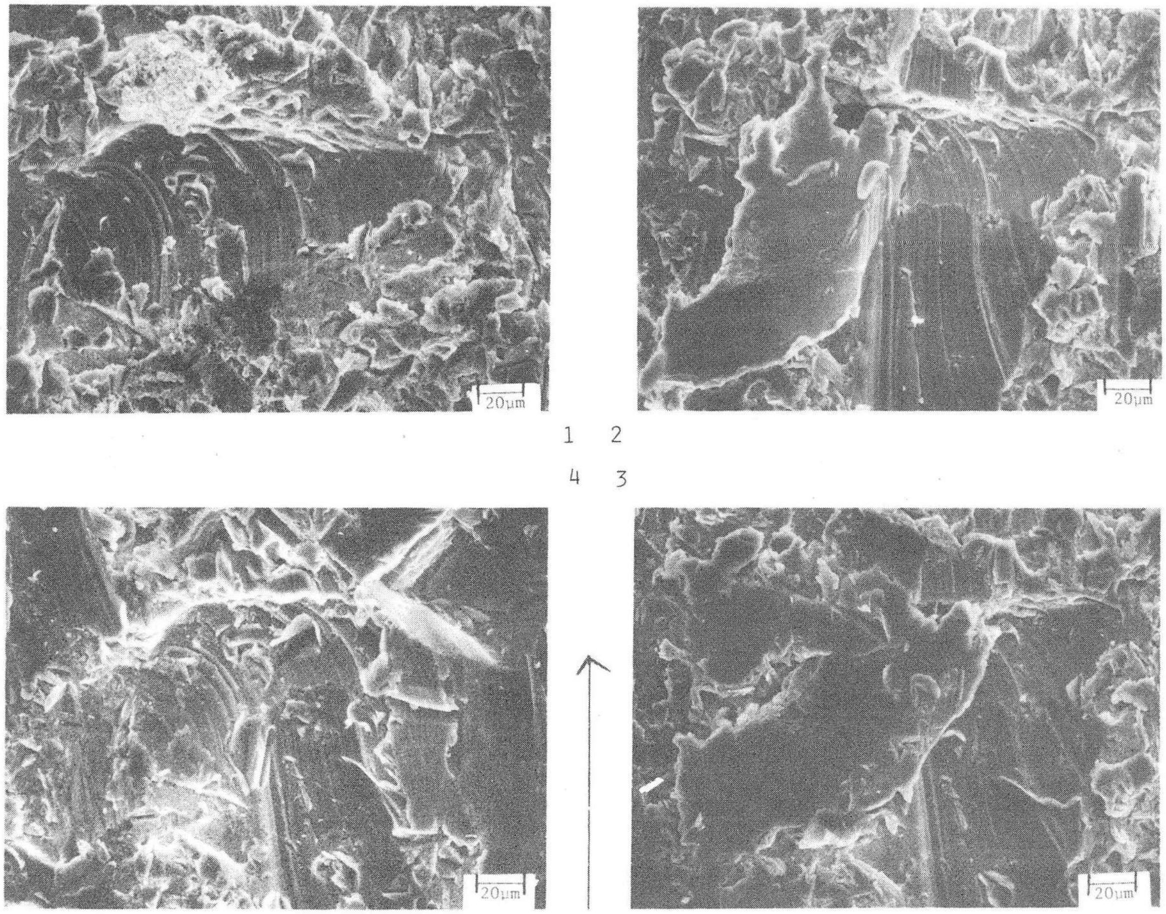

Fig. 13 Sequence of platelet formation and removal on 7075-T6 Al

XBB801-1299

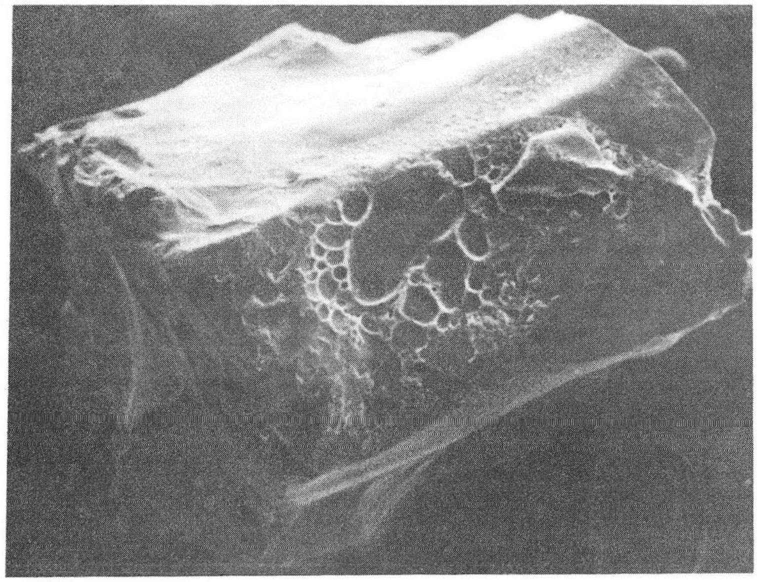

200 μm

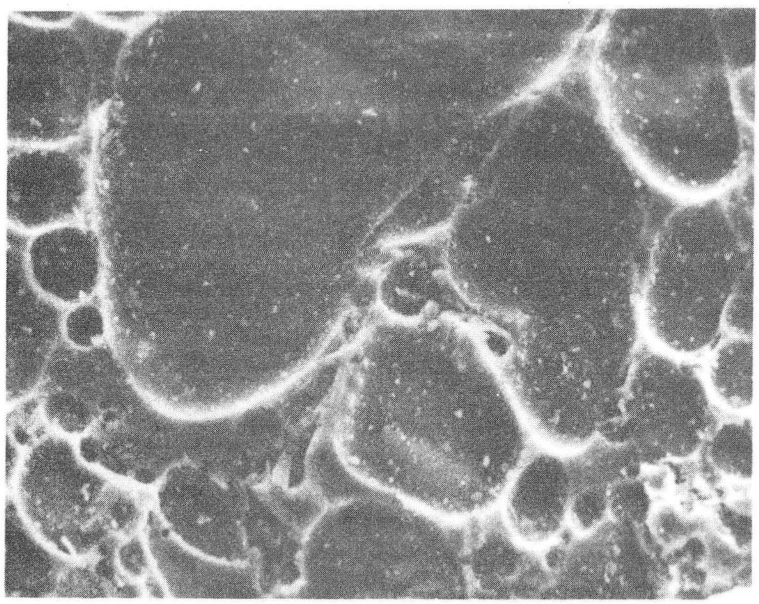

40 μm

Fig. 14 Melted and resolidified aluminum on a SiC erodent particle

XBB806-7863

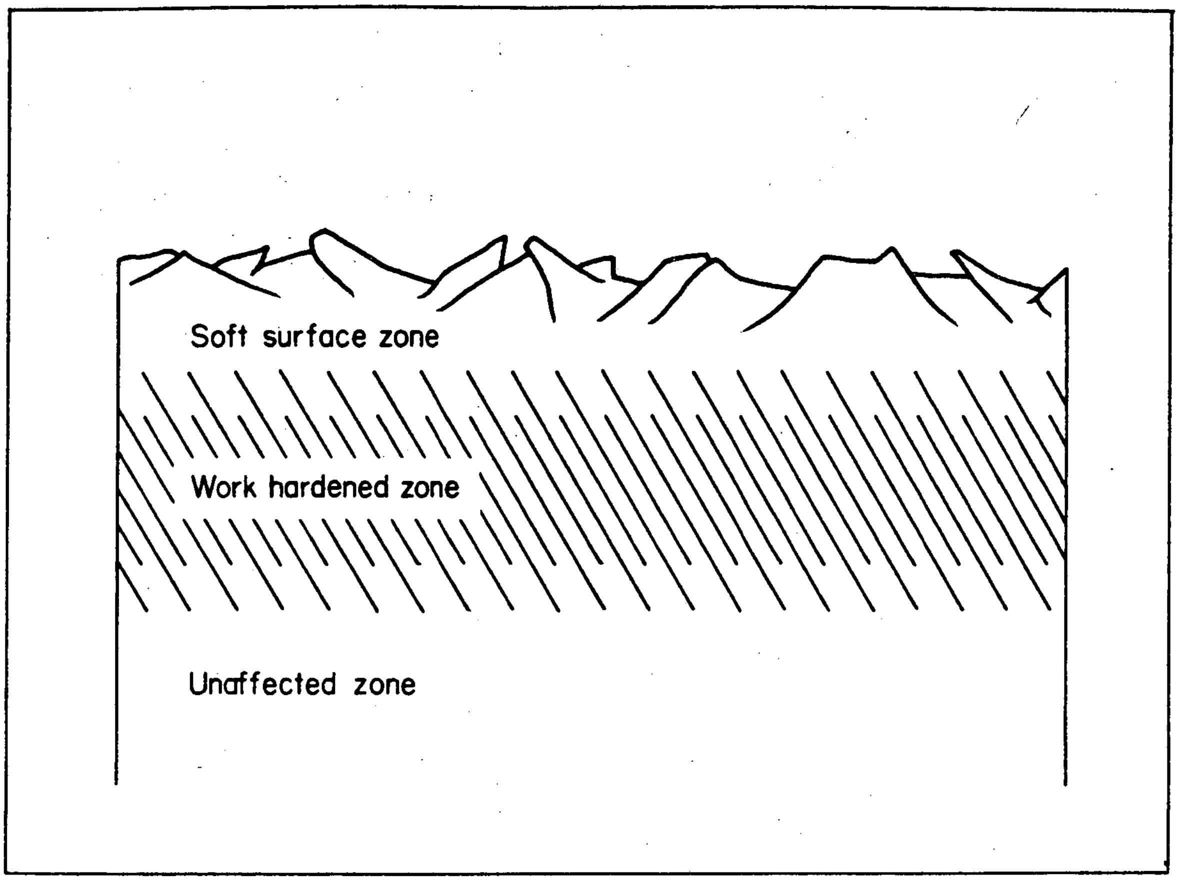

Fig. 15 Sketch of cross section of eroding metal surface

XBL807-10669

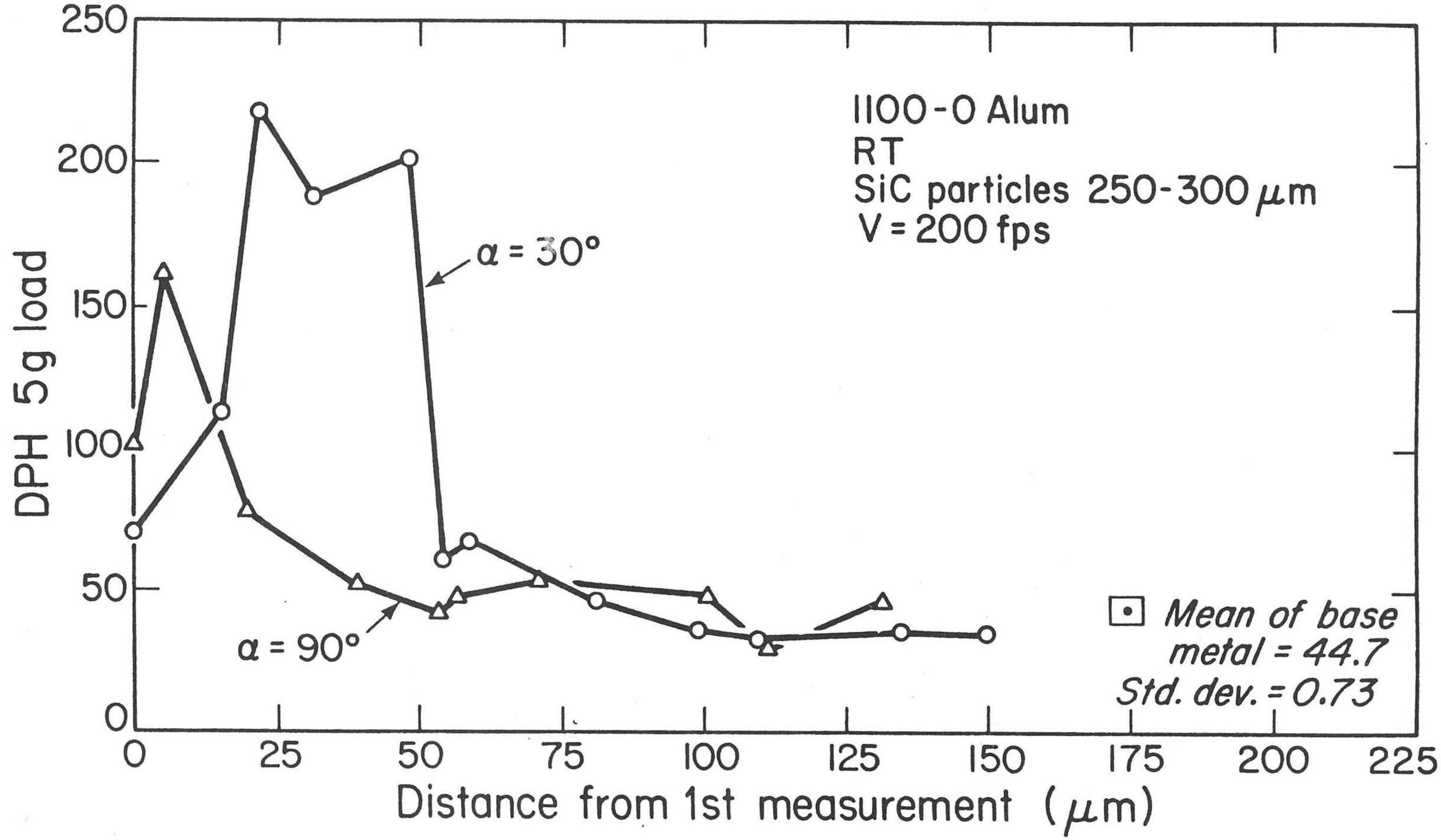

Fig. 16 Hardness survey across eroded material surface region

XBL 8011-2236

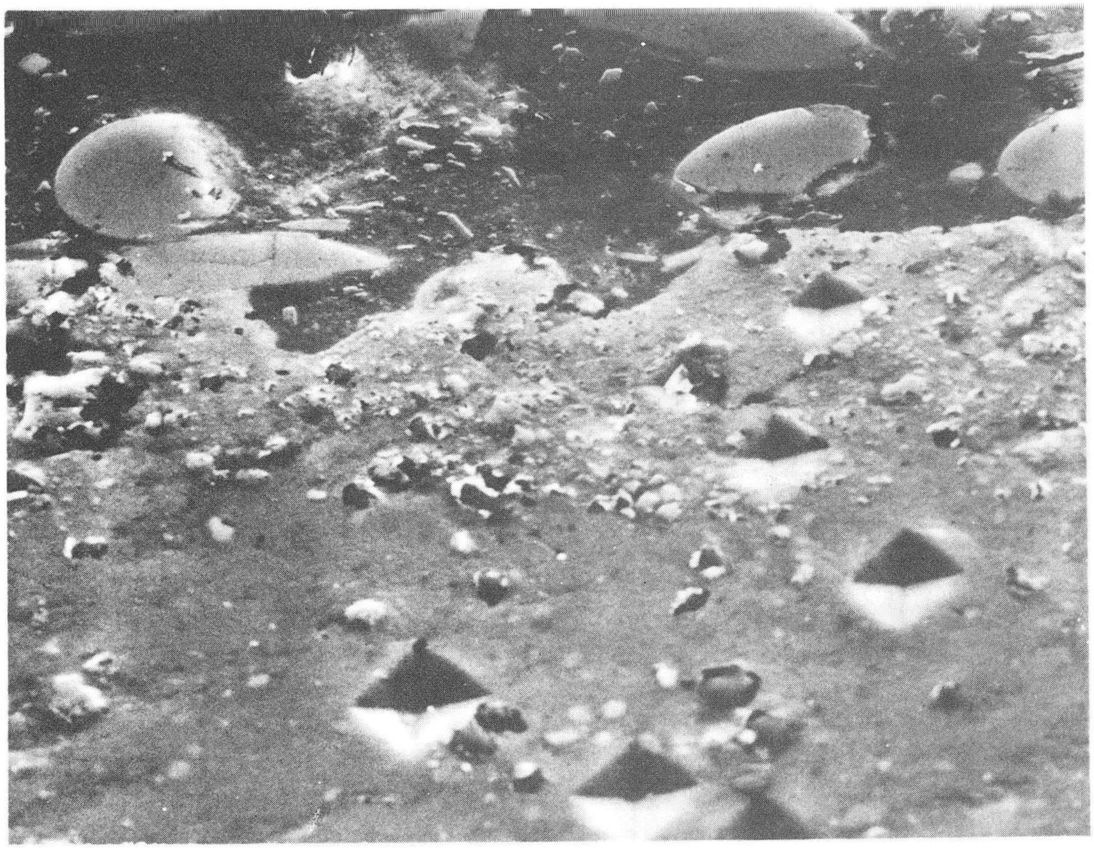

XBB 826-4982

1100-0 Al @ 1000X

10um

Fig. 17 Photo of micro-hardness indentations

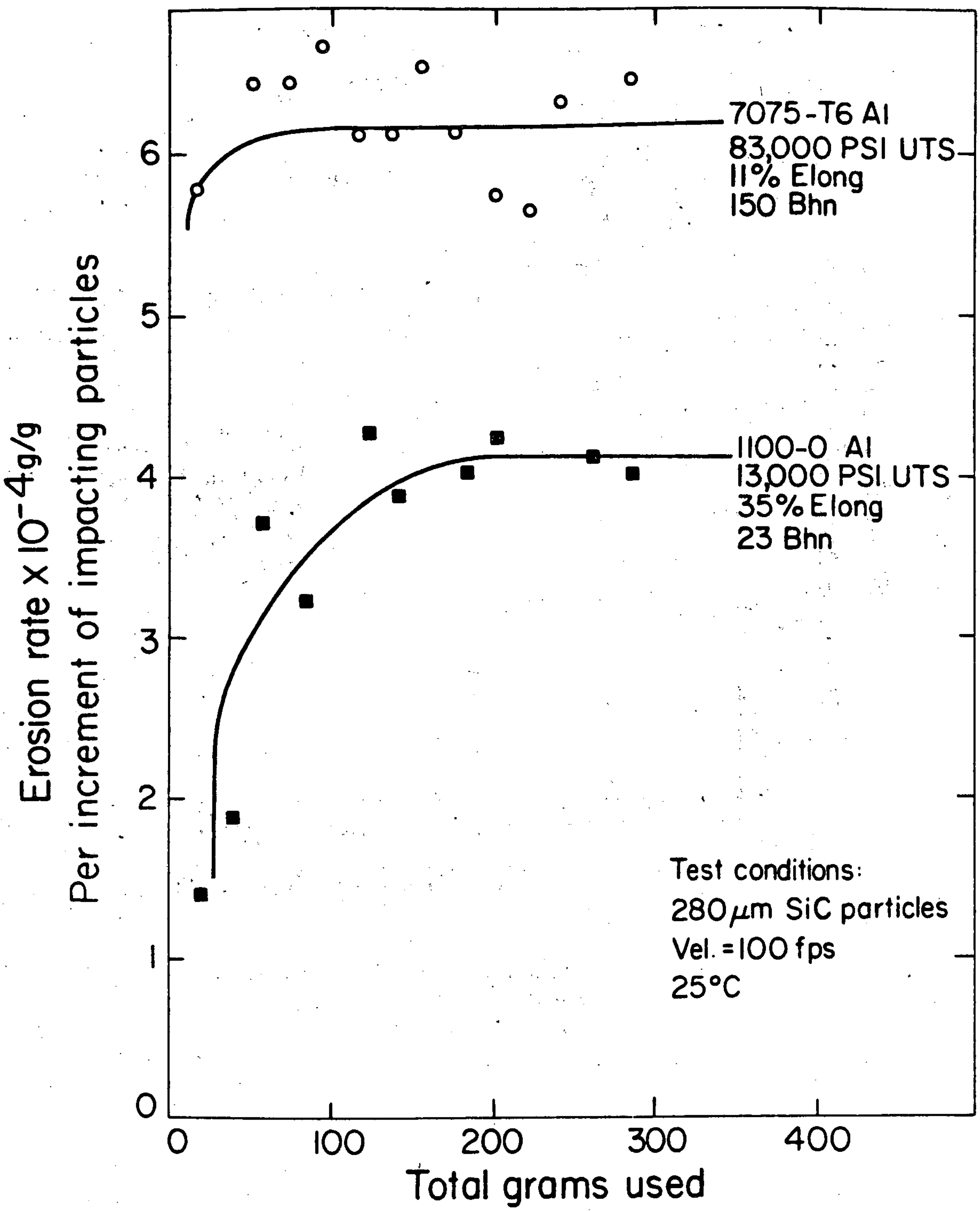

Fig. 18 Erosion rate of 7075-T6 and 1100-0 aluminum

XBL 8110-1379

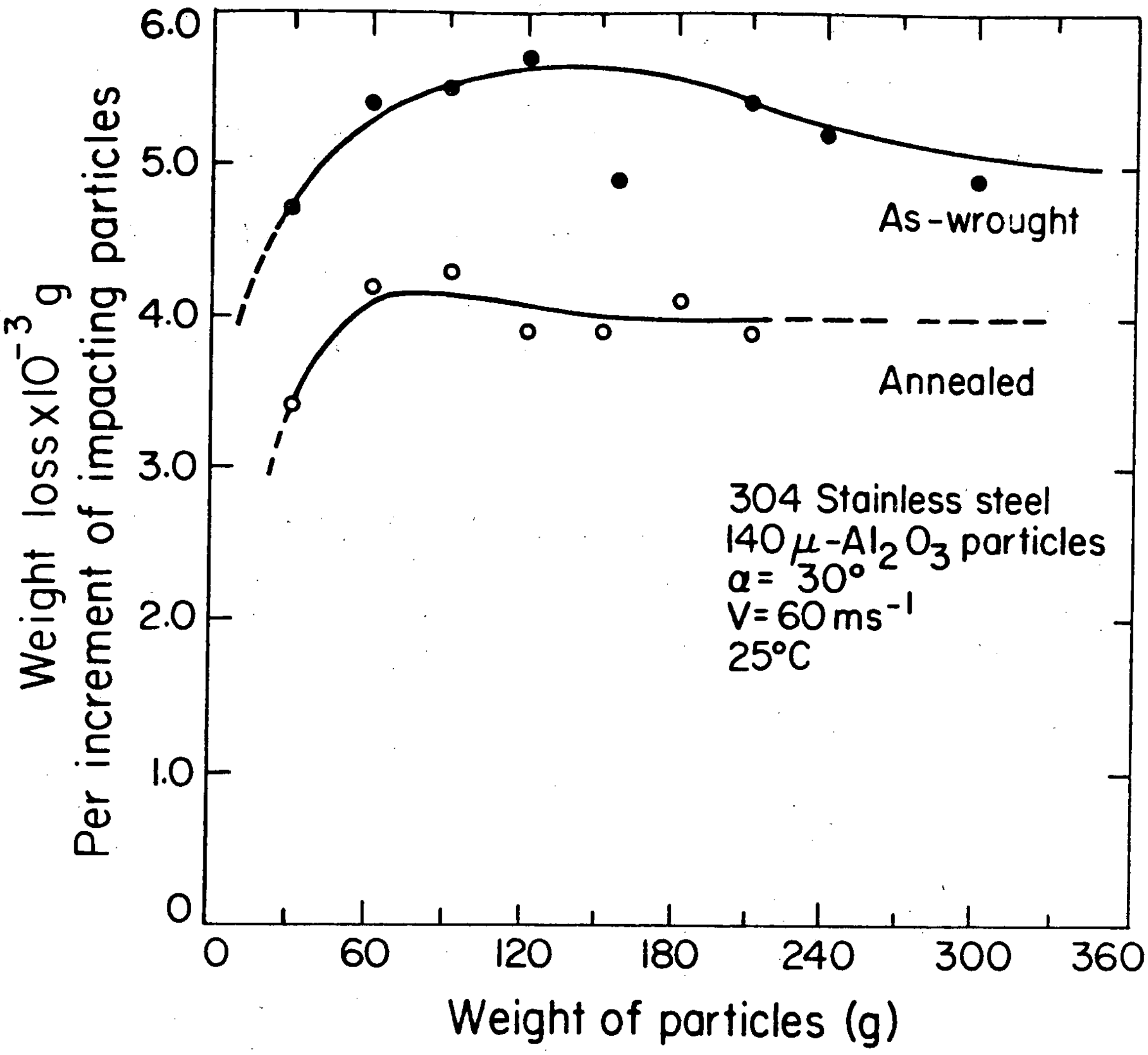

Fig. 19 Erosion rate of 304 stainless steel in as-wrought and annealed conditions

XBL 8110-1392

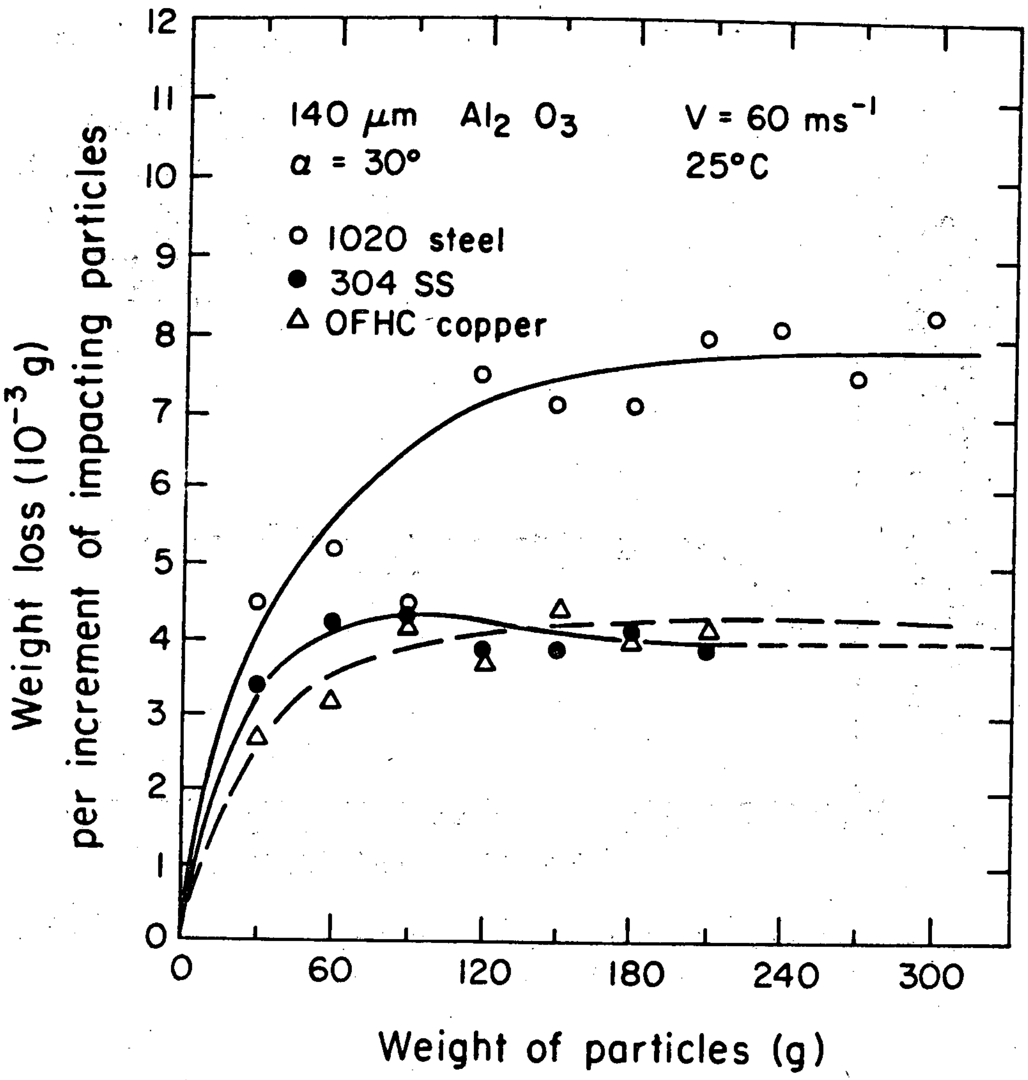

Fig. 20 Effect of Ductility on the Erosion of 1020 Steel and 304ss

XBL 829 – 1133

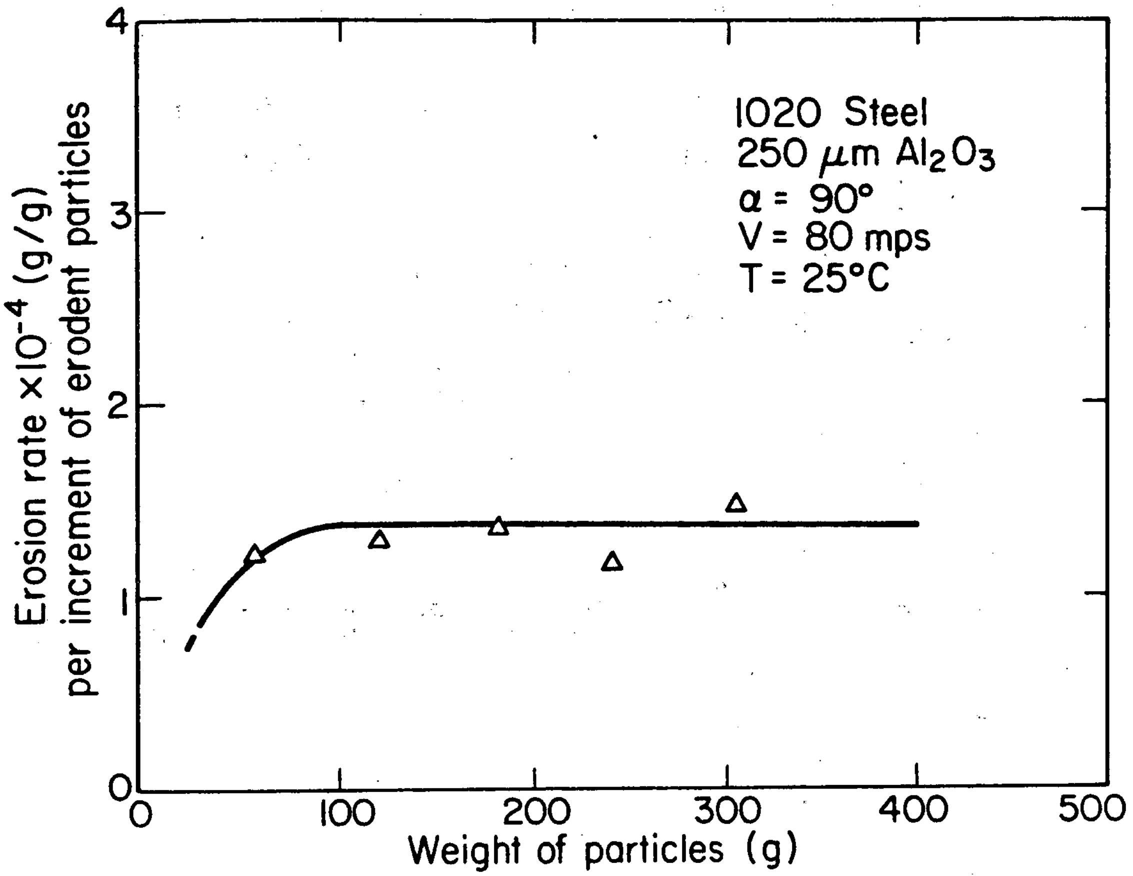

Fig. 21 Erosion rate of 1020 steel using Al_2O_3 particles

XBL 825-696

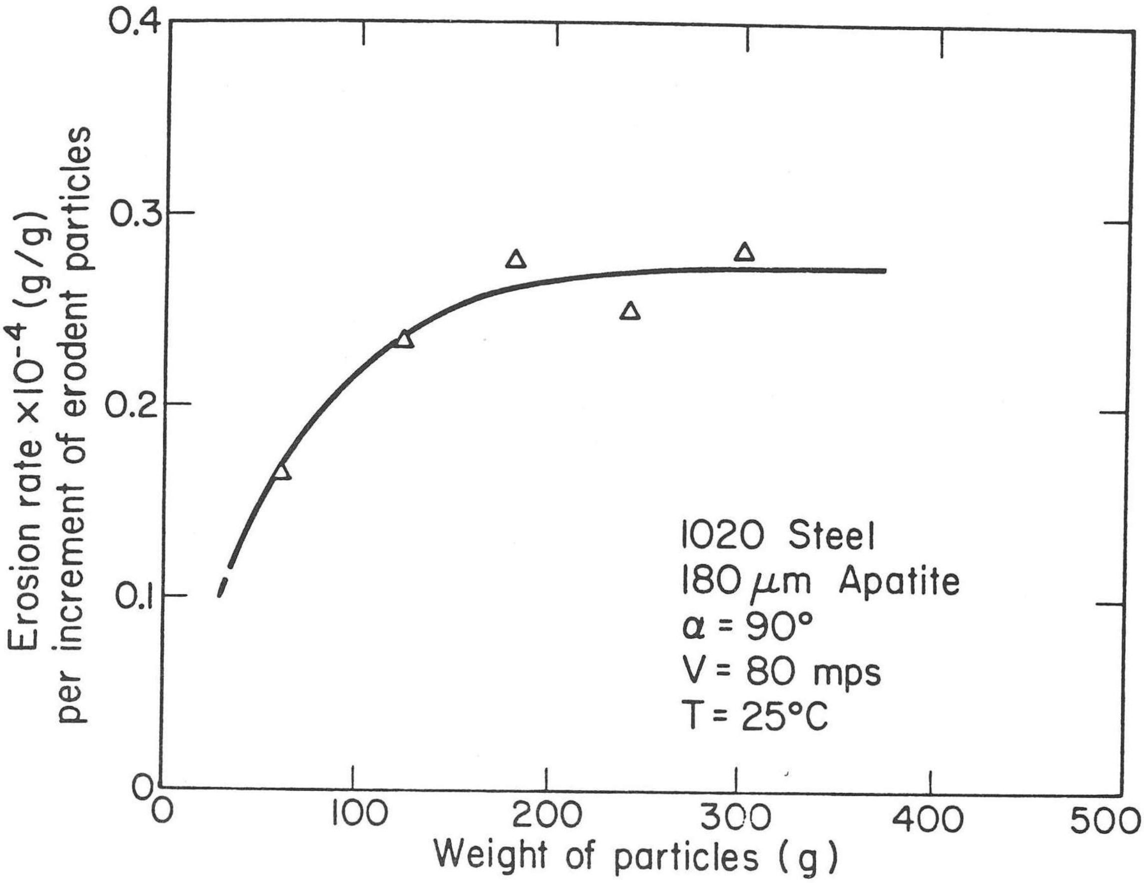

Fig. 22 Erosions rate of 1020 steel using apatite particles

XBL 825-694

Fig. 23 Cross section of delaminated 1075 steel eroded specimen

XBB775-5263

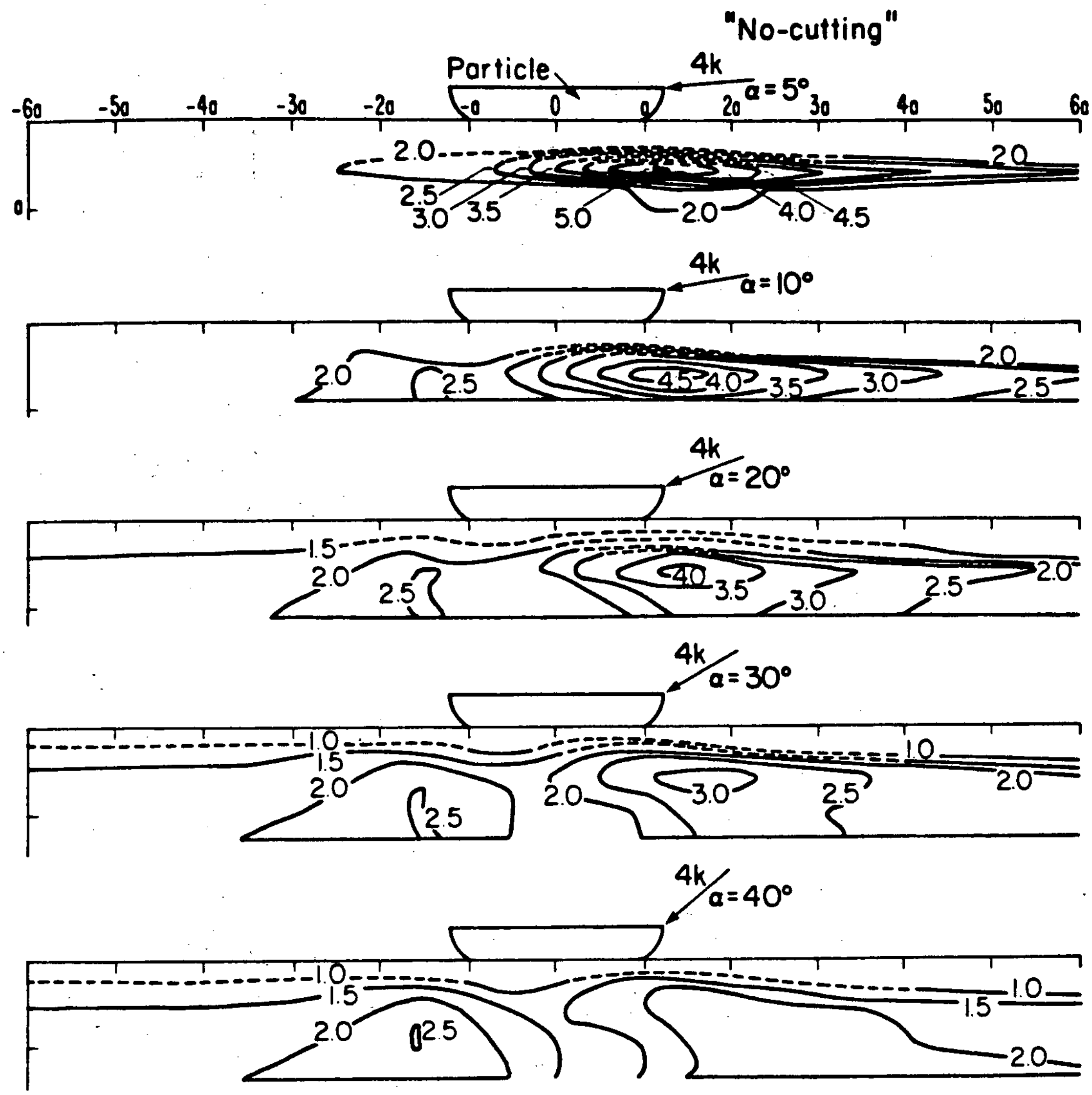

Fig. 24 Plots of critical shear stress areas beneath an impacting particle

XBL 793-818

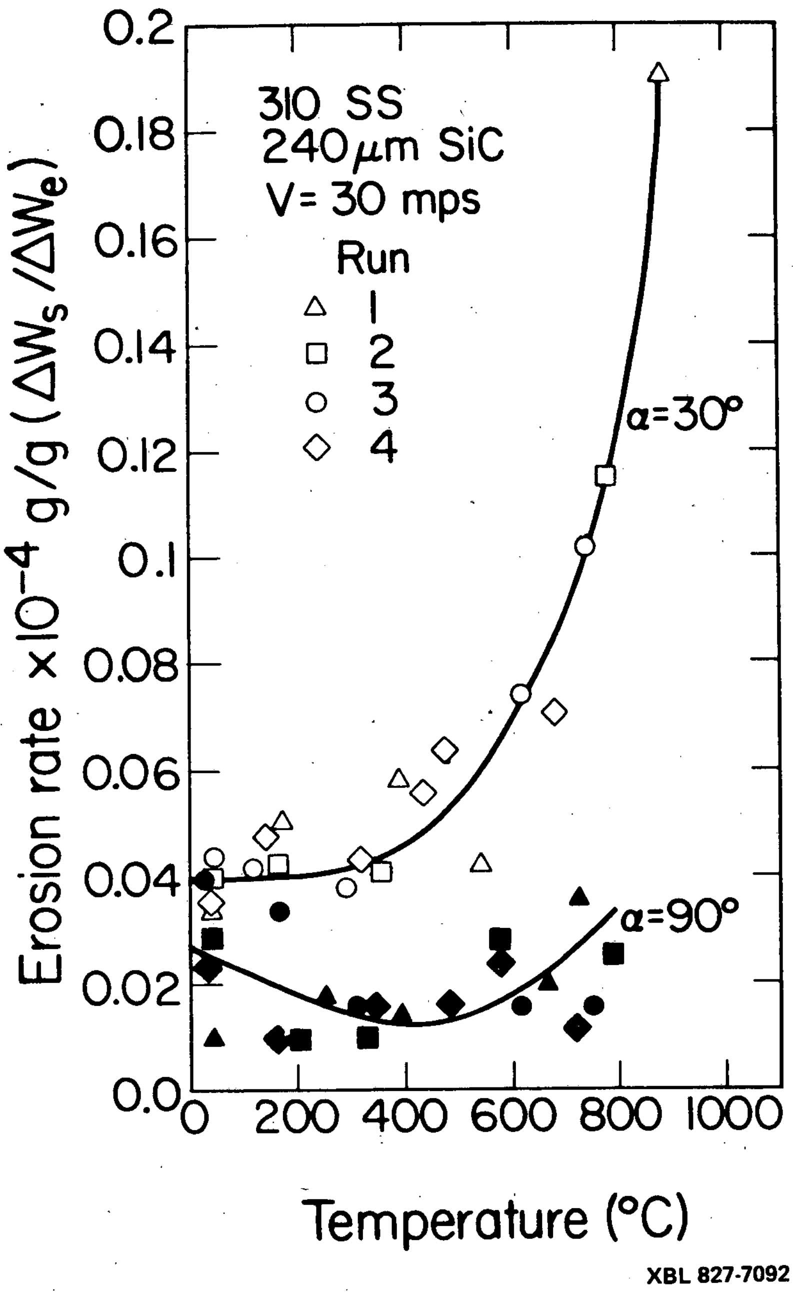

Fig. 25 Erosion rate of 310 SS at elevated temperature

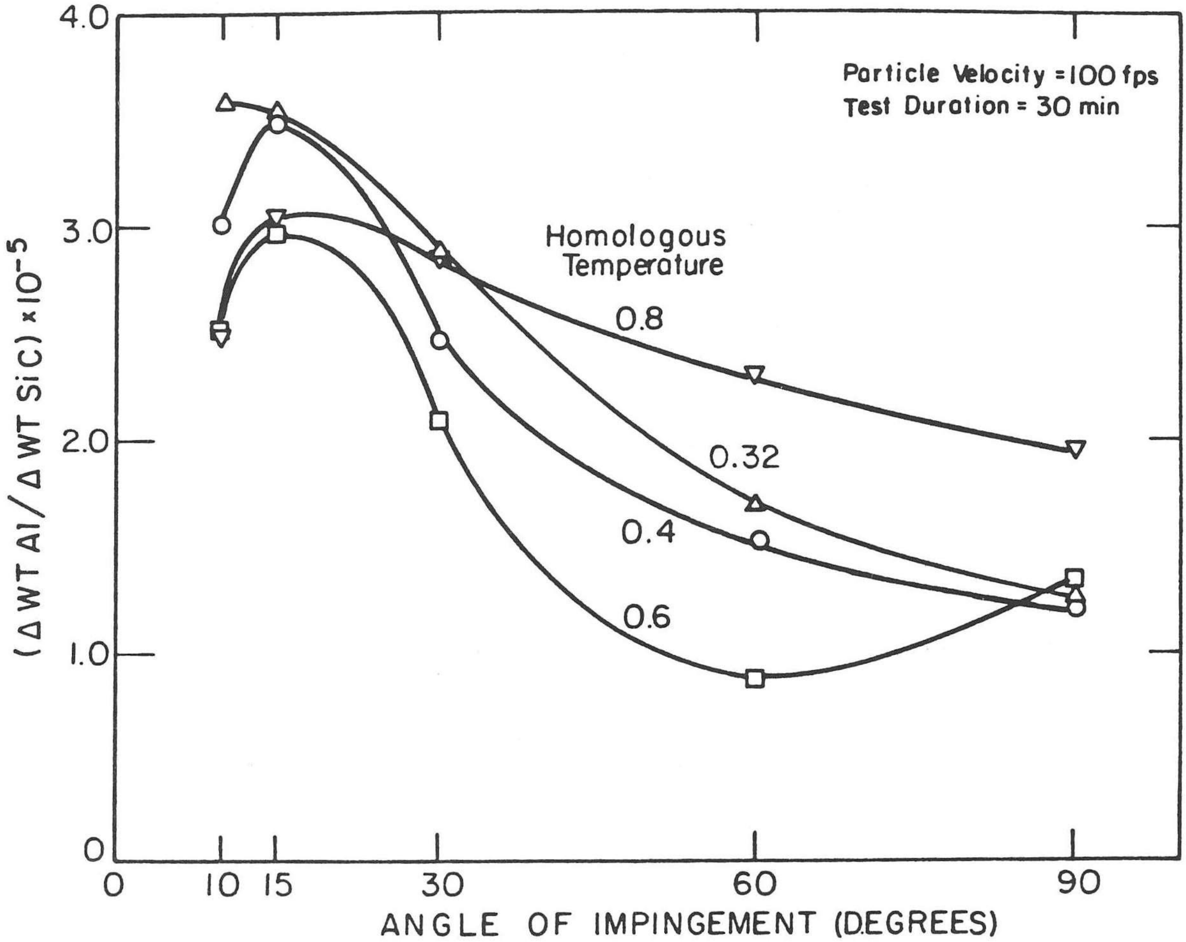

Fig. 26 Erosion rate of 1100-0 Al at various homologous temperatures

XBL778-5889

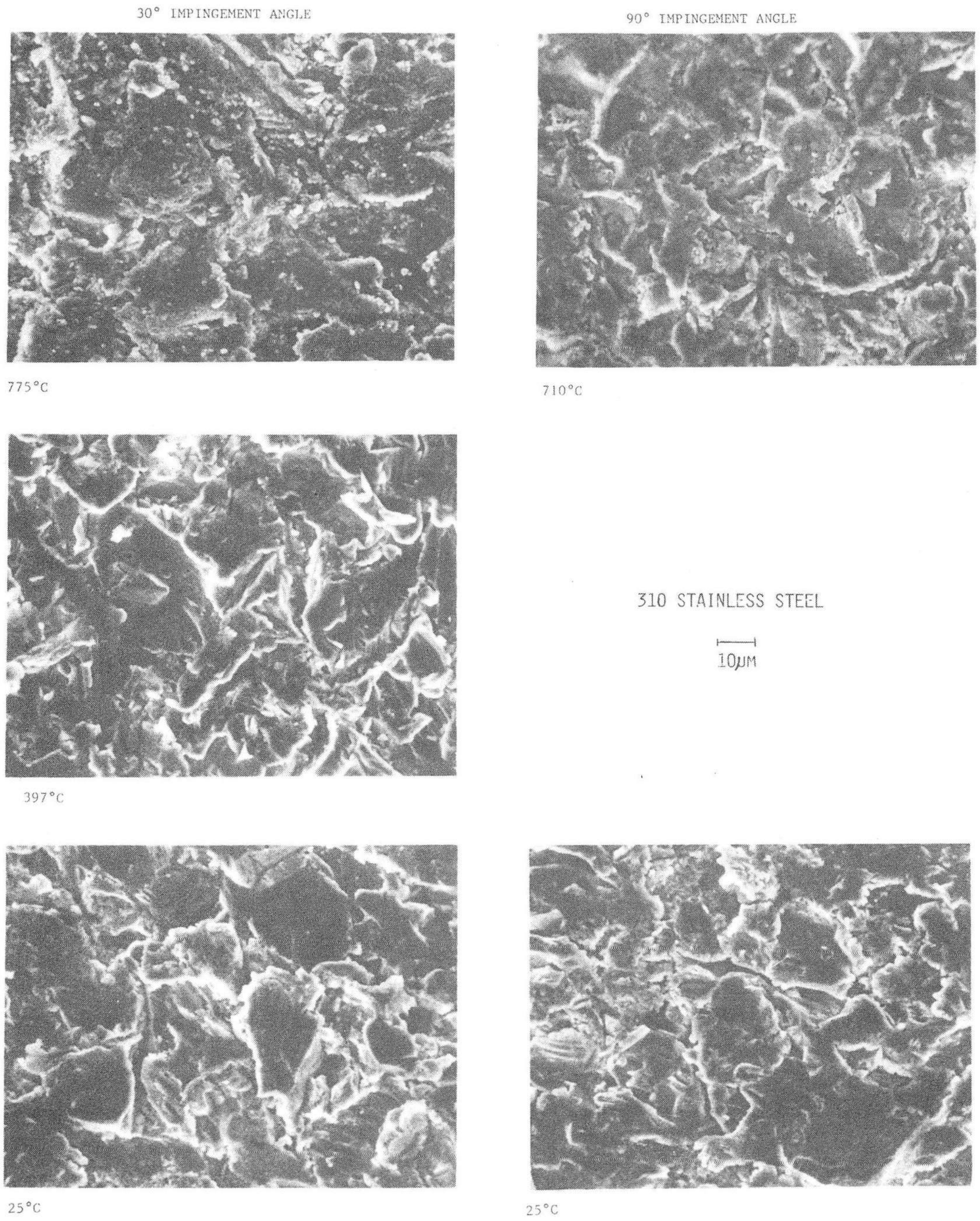

Fig. 27 Microstructure of 310SS surface at various test temperatures after erosion XBB824-3329

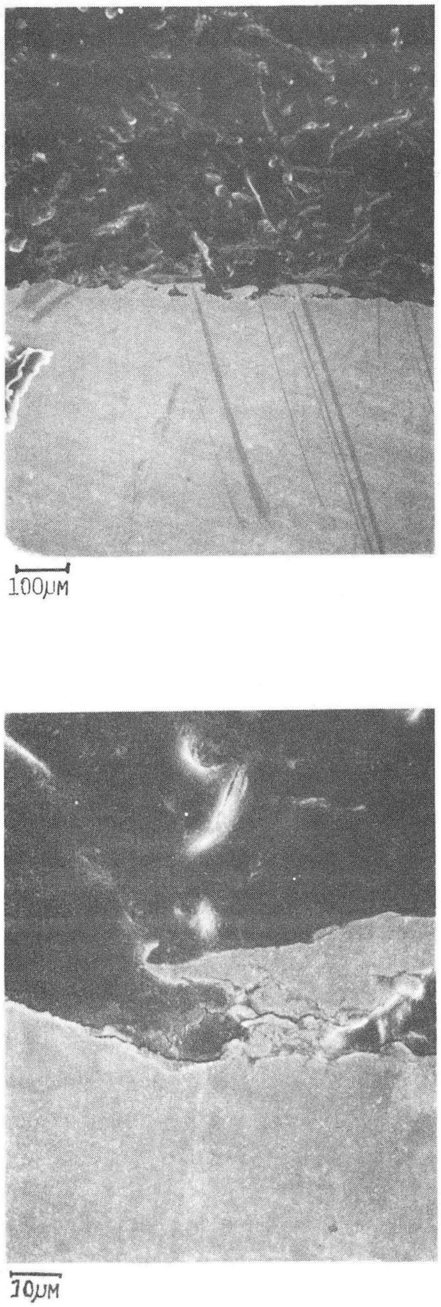

310 STAINLESS STEEL
30° IMPINGEMENT ANGLE
710°C
CROSS SECTIONAL VIEW

Fig. 28 Cross section of 310SS eroded surface showing platelets

XBB824-3330

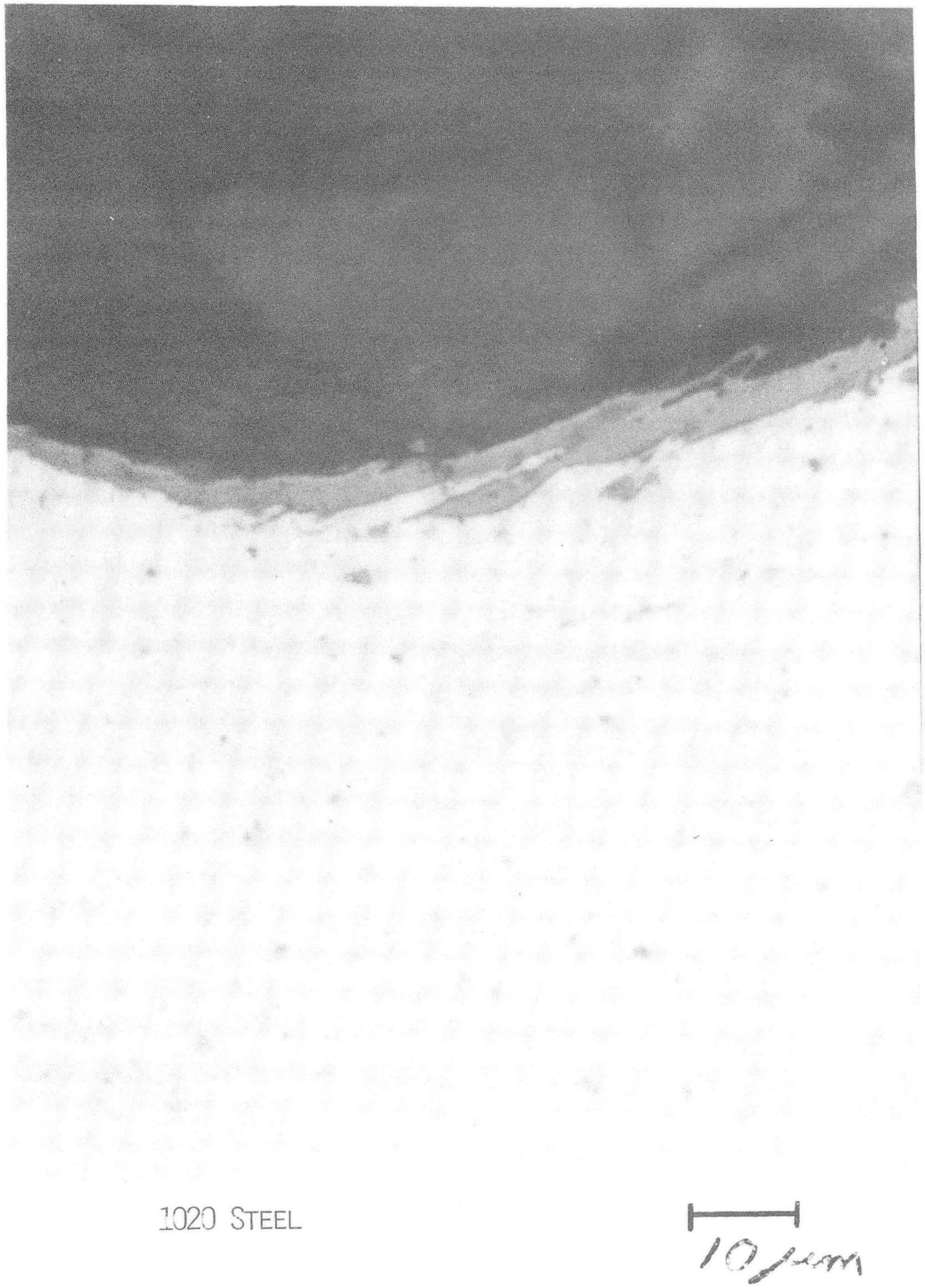

Fig. 29 Cross section of platelets formed on 1020 steel

XBB821-308

DISTRIBUTION LIST

Wate Bakker
EPRI
Hillview Ave.
Palo Alto, CA 94303

Susan M. Benford
NASA Lewis Research Center
21000 Brookpark Rd.
Cleveland, OH 41135

Mr. R.A. Bradley, Manager
Fossil Energy Materials Program
Oak Ridge National Laboratory
P.O. Box X
Oak Ridge, TN 37830

Richard Brown
Materials Durability Division
College of Engineering
University of Delaware
Newark, DE 19711

Dr. P.T. Carlson, Task Leader
Fossil Energy Materials Program
Oak Ridge National Laboratory
P.O. Box X
Oak Ridge, TN 37830

Mr. J.P. Carr
Department of Energy, Office of Fossil Energy
FE-42, Mailstop 3222-GTN
Washington D.C. 40525

Hans Conrad
Materials Engineering Department
North Carolina State University
Raleigh, NC 27607

Mr. S.J. Dapkunas
Department of Energy, Office of Fossil Energy
Technical Coordination Staff FE-14, Mailstop C-156 GTN
Washington D.C. 40525

DOE Technical Information Center
P.O. Box 62
Oak Ridge, TN 37830

Bill Ellingson
Argonne National Laboratory
9700 South Cass Ave.
Argonne, IL 60439

Mary Ellen Gulden
Solar Turbines International
PO Box 80966
San Diego, CA 92138

Mr. J.M. Hobday
Department of Energy
Morgantown Energy Technology Center
P.O. Box 880
Morgantown, WV 26505

Mr. E.E. Hoffman, Manager
National Materials Programs
Department of Energy
Oak Ridge Operations
P.O. Box E
Oak Ridge, TN 37830

Sven Jansson
Stal-Laval Turbin AB
Finspong S-61220
Sweden

Dr. R.R. Judkins
Fossil Energy Materials Program
Oak Ridge National Laboratory
P.O. Box X
Oak Ridge, TN 37830

Thomas Kosel
University of Notre Dame
Dept. of Metallurgical Engineering & Materials Science
Box E
Notre Dame, IN 46556

Mr. E.L. Long, Jr.
Fossil Energy Materials Program
Oak Ridge National Laboratory
P.O. Box X
Oak Ridge, TN 37830

Norman H. MacMillan
Pennsylvania State University
167 Materials Research Laboratory
University Park, PA 16802

Ken Magee
Bingham-Willamette Co.
2800 N.W. Front Ave.
Portland, OR 97219

Fred Pettit
Dept. of Metallurgy and Materials Engineering
University of Pittsburgh
Pittsburgh, PA 15261

Alberto Sagüés
IMMR — University of Kentucky
763 Anderson Hall
Lexington, KY 40506

Gordon Sargent
University of Notre Dame
Dept. of Metallurgical Engineering & Materials Science
Box E
Notre Dame, IN 46556

Paul Shewmon
Dept. of Metallurgical Engineering
116 W. 19th Ave.
Columbus, OH 43210

John Stringer
EPRI
3412 Hillview Avenue
P.O. Box 10412
Palo Alto, CA 94303

Widen Tabakoff
Dept. of Aerospace Engineering
University of Cincinnati
Cincinnati, OH 45221

Edward Vesely
IITRI
10 West 35th St.
Chicago, IL 60616

J.C. Williams
Dept. of Metallurgy & Materials Science
Carnegie-Mellon University
Schenley Park
Pittsburgh, PA 15213

Ian Wright
Materials Science Division
Battelle Memorial Institute
505 King Ave.
Colombus, OH 43201

TECHNICAL INFORMATION DEPARTMENT
LAWRENCE BERKELEY LABORATORY
UNIVERSITY OF CALIFORNIA
BERKELEY, CALIFORNIA 94720